Topics in Catalysis
https://doi.org/10.1007/s11244-026-02286-1

REVIEW PAPER

Femtosecond Absorption Spectroscopy to Elucidate Elementary Mechanisms of Molecules in Complex Environments

Maria Theresia Lahm[1,2] · **Andreas-Neil Unterreiner**[1]

Received: 13 February 2026 / Accepted: 29 March 2026

Abstract
Understanding the ultrafast dynamics of photoexcited molecules in complex environments is essential for advancing photochemistry, photocatalysis, and material design. These processes modulate excited-state pathways and ultimately determine product formation on longer timescales. This review presents how femtosecond broadband absorption spectroscopy, complemented by stationary spectroscopic techniques, reveals elementary processes such as internal conversion, intersystem crossing, and charge transfer—often mediated by conical intersections and influenced by solvent dynamics. Case studies span vision-related isomerization to several structurally and mechanistically distinct photocatalytic systems. They highlight the decisive role of intra- and intermolecular interactions, e.g., those mediated by non-innocent ligands and surrounding media. Special attention is given to the Red-Edge effect, where excitation wavelength-dependent reactivity challenges conventional photophysical and -chemical assumptions. By correlating ultrafast spectroscopy with quantum chemical calculations and complementary long-timescale methods, we obtain mechanistic insight into excited-state behavior. This knowledge shows how molecular structure and environment govern photoreactivity and enables rational design of photoactive and functional materials.

Keywords Femtosecond spectroscopy · Ultrafast dynamics · Photoexcited states · Red-Edge effect · Fundamentals of photocatalysis

1 Introduction

Photochemical processes underpin a broad spectrum of natural and technological phenomena, spanning visual perception to solar energy conversion [1, 2]. Elementary molecular events unfold on femtosecond (fs) to picosecond (ps) timescales and ultimately determine the fate of photoexcited states. Achieving a detailed understanding of such ultrafast dynamics in realistic, complex environments is therefore crucial for advancing photochemistry, photocatalysis and the rational design of photoactive materials [3]. While Eigen, Norrish and Porter were awarded the Nobel Prize in 1967 for achieving microsecond (μs) time resolution in chemical reactions [4–9], direct access to elementary excited-state dynamics became feasible only with the advent of fs laser technology [10–22]. As early as 1988, Ahmed H. Zewail articulated the fundamental challenge of modern photochemistry by emphasizing that chemical bond breaking and formation occur with extraordinary speed in the transition-state region, where the entire reaction pathway—including product distribution—is defined [16]. Zewail's pioneering work, which enabled real-time observation of bond formation and cleavage on atomic timescales, marked a paradigm shift in chemical dynamics and was awarded the 1999 Nobel Prize. This realization established that ultrafast dynamics govern the branching between radiative, non-radiative, and reactive channels [15, 16, 23–25].

The ultrafast dynamics of photoexcited molecules are often governed by conical intersections, which facilitate rapid non-radiative transitions between electronic states. A landmark demonstration was reported by Polli et al. [1], who showed that the retinal isomerization underlying vision proceeds via a conical intersection within appr.

✉ Andreas-Neil Unterreiner
andreas.unterreiner@kit.edu

[1] Institute of Physical Chemistry, Karlsruhe Institute of Technology (KIT), Kaiserstr. 12, 76131 Karlsruhe, Germany

[2] Institute of Functional Interfaces, Karlsruhe Institute of Technology (KIT), Hermann Von Helmholtz Platz 1, 76344 Eggenstein-Leopoldshafen, Germany

Published online: 29 April 2026

200 fs, with coherent wave-packet motion tracked using sub-20 fs spectroscopy [1]. Such studies underscore that only spectroscopic techniques with fs temporal resolution can directly capture these fleeting, yet decisive, molecular events. In realistic systems, excited-state dynamics are not dictated solely by intrinsic molecular properties. Intra- and intermolecular interactions, together with environmental factors such as solvent dynamics, critically modulate the rates and competition of individual pathways, thereby shaping excited-state branching [10, 26–28]. Developing a mechanistic understanding of these influences is essential for formulating design strategies that enable targeted control over photochemical reactivity and efficiency. Over the past decades, fs transient absorption spectroscopy (TAS) has emerged as a key experimental tool for probing such processes in real time [29]. It allows direct observation of elementary steps including internal conversion (IC), intersystem crossing (ISC) and charge transfer (CT) following photoexcitation. At the same time, interpreting fs TAS data in complex molecular systems remains challenging, as multiple transient contributions often overlap. Already in 1990, Khundkar et al. [10] recognized that a comprehensive description of ultrafast reaction dynamics requires integration of time-resolved techniques with complementary stationary methods.

These concepts are pertinent to photocatalysis, where efficiency and selectivity are frequently determined within the first few fs after excitation [29, 30]. Early work by Damrauer et al. [31] demonstrated that the identity and distribution of photochemical products are governed by ultrafast photophysical processes, highlighting the central role of ultrashort-timescale spectroscopy in elucidating modern photoredox mechanisms [30]. A particular emphasis of this Review is placed on excitation-wavelength-dependent phenomena, most notably the so-called Red-Edge effect [32–37]. Originally identified in fluorescence spectroscopy, it is becoming increasingly evident that excitation-wavelength-dependent reactivity also plays a decisive role in photochemistry, challenging long-standing assumptions such as excitation-independent emission or maximal reactivity at peak absorption [38–57]. Combined action-plot analysis and ultrafast spectroscopic measurements reveal that processes such as fluorescence or ISC can critically influence quantum yields when they occur on timescales faster than solvent relaxation [43].

This review builds upon the plenary lecture delivered by the corresponding author at the 10th National Catalysis Conference (NCC-10) (Sivas Cumhuriyet University, 2025), focusing on fs TAS as a powerful tool for unraveling elementary mechanisms in photoexcited molecules. We explore how molecular structure and environmental factors modulate these mechanisms and how this knowledge can be leveraged for rational material design. Our experimental approach combines fs broadband TAS with stationary spectroscopic and electrochemical techniques, complemented by quantum-chemical calculations. Systematic variation of ligands, solvents, chromophoric units, excitation conditions and reference systems enables correlations between time-resolved observables—such as excited-state lifetimes—and stationary properties including absorption characteristics and quantum yields. This integrative strategy provides mechanistic insight into complex excited-state landscapes and forms a foundation for the rational design of future photoactive materials.

This review does not aim to comprehensively assess the extent to which ultrafast spectroscopic methods have already been adopted in photocatalysis, nor to establish a unified methodological or mechanistic framework for the field. Instead, we present selected case studies that exemplify the current state of research and highlight the insight afforded by ultrafast spectroscopy. These examples range from vision-related isomerization [1] to structurally and mechanistically diverse photocatalytic systems, illustrating the breadth of excited-state dynamics and reactivity patterns encountered in photochemistry. Individual electron-transfer mechanisms are addressed only in brief, as they constitute a broad and well-established research field beyond the scope of this review. Detailed treatments of the fundamental principles of electron-transfer in photocatalysis, along with recent developments, are available in numerous dedicated studies, including those by Pfund et al. [58, 59], Balapure et al. [60], Lee et al. [61] and Sakizadeh et al. [30].

2 Experimental Approach and Spectroscopic Techniques

Photon absorption enables selective population of electronically excited states of a molecule [62, 63], with the photon energy defined by its frequency according to the Planck-Einstein relation [64–66]. The quantitative characterization of molecular absorption is given by the Beer-Lambert law [67–69], where the absorption strength of a sample is expressed in terms of the molar decadic absorption coefficient [62, 63, 70]. However, the evaluation of transition probabilities and intensities necessitates a quantum mechanical treatment based on perturbation theory [62, 63, 71], wherein the molecular absorption rate depends on the magnitude of the transition dipole moment within the framework of Fermi's golden rule [63, 64, 72, 73]. In practice, transition dipole moments are often rarely known with sufficient precision to reliably predict the branching behavior of a molecule in its excited state. As a result, a comprehensive understanding of molecular excited-state dynamics necessitates the

application of multiple, complementary experimental and theoretical techniques.

Following optical excitation into an electronically excited singlet state (S_1 or S_n), molecular deactivation can proceed via radiative and non-radiative relaxation pathways, as well as through CT or photochemical reaction (CR) [10, 63, 74, 75]. The interplay between these competing processes is commonly depicted using a Jabłoński diagram (Fig. 1) [76]. Among the earliest non-radiative events are vibrational relaxation (VR) and intramolecular vibrational redistribution (IVR), which dissipate excitation energy through inter- and intramolecular channels on timescales spanning hundreds of fs to nanoseconds (ns) [10, 74, 77]. Exited-state evolution is further governed by isoenergetic transitions between electronic states. IC connects states of identical spin multiplicity and typically occurs on ps to sub-µs timescales [75, 77], whereas ISC mediates spin-forbidden transitions between singlet and triplet manifolds, extending from ps to µs. The reverse process (rISC) may proceed on substantially longer timescales, reaching the millisecond (ms) regime [75, 78]. Although ISC is formally spin-forbidden, it becomes weakly allowed through spin–orbit coupling, which can be enhanced by heavy atoms or specific functional groups [77, 78]. Due to the high density of vibrational and rotational states at elevated energetic regions, population of higher electronic states is typically followed by rapid non-radiative relaxation to the fundamental vibration level of the lowest excited singlet or triplet state. The comparatively large energy gap between S_1 and the electronic ground state S_0, combined with reduced non-radiative transition probabilities in accordance with the Franck–Condon principle, renders radiative decay competitive. In agreement with Kasha's rule [79], emission generally originates from the fundamental vibration level of the lowest excited state and is independent of the excitation wavelength, although well-established exceptions exist [10, 62, 75, 77, 80]. Radiative deactivation occurs either via fluorescence, which preserves spin multiplicity and exhibits lifetimes in the ns to sub-µs range [81], or via phosphorescence, which involves spin-forbidden transitions and may persist from µs to hours [63, 72, 75, 81, 82]. Beyond relaxation pathways, photoexcitation can initiate CT processes or trigger CR that are central to the function of photoactive systems [2, 74, 76].

The overall efficiency of such photochemical processes is dictated by the competition between productive pathways leading to reactive intermediates or final products and dissipative loss channels that deactivate the system [30]. A central method for probing excited-state dynamics is fs pump-probe spectroscopy. In this approach, an ultrashort laser pulse is divided into a pump pulse that initiates photoexcitation and a time-delayed probe pulse that monitors transient changes in absorption of the excited sample. Systematic variation of the delay time allows recording of the temporal evolution of the system in the form of TA spectra, defined as probe-pulse absorption with and without pump-pulse excitation [2, 18, 29]. In fs broadband TAS, the probe spans a wide spectral range, enabling real-time observation of transient species and electronic transitions following photoexcitation. Detailed experimental implementations are reported elsewhere [83–85]. The resulting transient spectra contain characteristic signatures of distinct processes: negative transient responses arise from ground-state bleaching (GSB) or stimulated emission (SE), while positive contributions are associated with excited-state absorption (ESA)

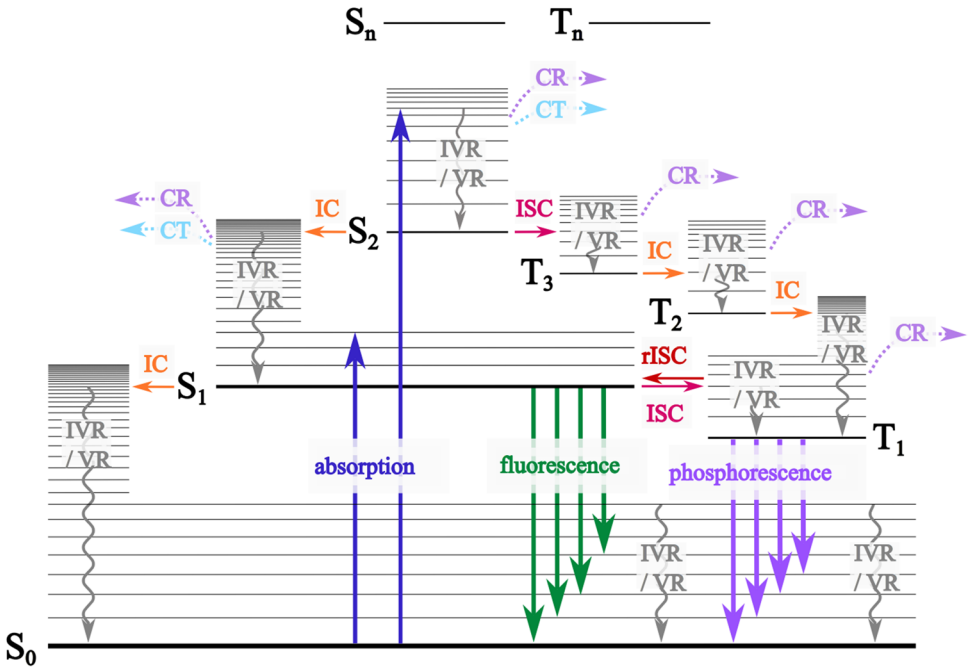

Fig. 1 Jabłoński diagram illustrating fundamental photophysical und -chemical processes that can occur after optical absorption. See text for further explanations

or hot ground-state absorption (HGSA). An ultrafast photochemical reaction leads to various photoinduced species such as intermediates, whose dynamics can also be mapped [2, 20, 29, 85]. In complex systems, these contributions frequently overlap, complicating unambiguous pathway assignment [20, 85]. Consequently, comprehensive mechanistic insight necessitates the integration of ultrafast spectroscopy with complementary steady-state techniques and theoretical modeling. UV–Vis and fluorescence spectroscopy, NMR and EPR for long-timescale dynamics and quantum-chemical calculations for electronic structure and excited-state pathways provide essential contextual information. Complementary, action plots—acquired using wavelength-tunable ns-pulsed lasers with constant photon flux at each wavelength—[43] correlate photochemical conversion yields with excitation wavelength, thereby directly linking optical absorption to chemical reactivity [86, 87]. Only through the integrative analysis of ultrafast, stationary and theoretical data, the branching pathways of complex excited-state dynamics can be resolved and their causal interdependencies elucidated, fulfilling the central objective of modern time-resolved spectroscopy.

3 Case Studies

3.1 Resolving Primary Ultrafast Vision-Related Isomerization Pathways by TAS

In line with seminal investigations of the cis–trans isomerization of retinal in rhodopsin, a process fundamental to visual perception [88–90], we correlate fs spectroscopic results, i.e., understanding the role of ultrafast dynamics such as IC – including conical intersections – and solvent dynamics in modulating reaction pathways and long-term behavior. Retinal photoisomerization is mediated by a conical intersection between the potential energy surfaces of the electronic ground and excited states and unfolds on an exceptionally fast timescale of about 200 fs [1, 91–94]. Resolving such dynamics experimentally requires techniques offering both high temporal resolution and broad spectral coverage. Early transient absorption studies [95, 96] employing ps time resolution identified intermediates and photoproducts, yet were intrinsically unable to directly access the primary sub-ps dynamics that determine photoproduct formation [97]. Accurately capturing the temporal evolution of such ultrafast processes therefore demands experimental timescales that commensurate with the underlying dynamics, i.e., the use of fs optical pulses [10, 11, 98–100]. Experiments employing sub-35 fs pulses [92] revealed that the cis–trans isomerization proceeds from a vibrationally coherent excited state and occurs on a timescale faster than typical vibrational dephasing and relaxation, comparable to the vibrational period of low-frequency torsional modes in retinal. This ultrafast behavior challenged the classical photochemical model, which assumes complete intrastate relaxation of the excited state prior to IC to the ground-state photoproduct. Instead, a nearly barrierless, nonadiabatic transition, governed by strong coupling between the excited state and the photoproduct ground state, was proposed [92, 97, 101], and further supported by theoretical studies describing a conical intersection between the ground- and excited-state potential energy surfaces [102, 103]. Polli et al. [1] provided direct experimental evidence of this mechanism (Fig. 2) using sub-20 fs broadband TAS, complemented by advanced molecular simulations. Collectively, these studies demonstrate that ultrafast broadband TAS constitutes a powerful and indispensable framework for resolving primary photoinduced processes on their intrinsic timescales. In combination with complementary approaches such as advanced theoretical simulations, it enables a comprehensive mechanistic understanding.

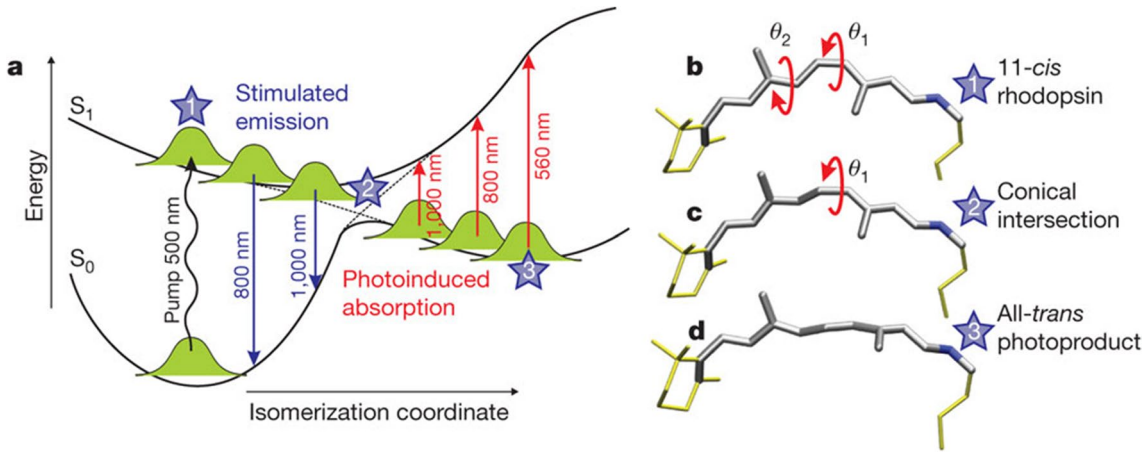

Fig. 2 **a** Isomerization potential energy surfaces of the chromophore in rhodopsin as a function of the isomerization coordinate. **b**–**d** Averaged structures of the chromophore during the cis–trans isomerization [1]. Reproduced from Polli D et al. [1] with permission from Springer Nature

3.2 Ultrafast Excited-State Dynamics Guiding Photochemical Efficiency

Studies [85, 104, 105] on photoinitiators for laser-induced polymerization provide a compelling demonstration of how ultrafast excited-state dynamics decisively shape subsequent processes and directly govern macroscopic reaction outcomes. In photoinitiated chain-growth polymerizations, both the initiating species and the propagating chain ends act as reactive centers, e.g. as radicals [104, 106–111]. However, in radical polymerization the initiation efficiency is not dictated solely by the chemical identity of the generated radicals, but is critically controlled by the elementary photophysical events occurring within the first few ps following photoexcitation, i.e., before radical formation [104, 105]. For efficient triplet-radical photoinitiation, rapid population of a triplet state from an excited singlet state via ISC is essential. This requires suppression of competing ultrafast non-radiative decay channels from the excited singlet state and a sufficiently small singlet–triplet energy gap [3, 112–118]; the resulting T_1 state must persist long enough to outcompete deactivation processes such as phosphorescence and enable productive radical formation [85]. Wolf et al. [85] conducted comparative studies on benzoin-type (benzoin (Bz) and 2,4,6-trimethylbenzoin (TMB)) and benzil-type (mesitil (Me)) photoinitiators, combining fs TAS with quantum-chemical calculations. This integrated approach allowed the authors to disentangle the mechanistic pathways governing population of the T_1 state and to correlate the resulting efficiency ratios quantitatively with photoinitiation efficiencies obtained from pulsed laser polymerization/electrospray ionization-mass spectrometry (PLP/ESI–MS) experiments, thereby providing a molecular-level rationale for the pronounced differences in photoinitiator efficiency. The benzoyl radical derived from Bz exhibits the highest initiation efficiency, whereas the mesitoyl radical displays strikingly different efficiencies depending on whether it is generated from TMB or Me. Despite the significantly stronger absorption of Me at the excitation wavelength, radicals generated from TMB outperform those from Me, even when TMB and Bz are excited nearly non-resonantly at the red edge of their weak absorption band (Fig. 3a) [85, 104, 105]. These observations demonstrate that high absorption at the excitation wavelength does not necessarily correlate with efficient photoinitiation. Instead, selective population of suitable electronic states and efficient ISC were identified as decisive factors: The combination of fs-TAS with excited-state calculations revealed that benzoin-type photoinitiators undergo rapid ISC from the initially populated S_1 state on sub-ps to ps timescales (Fig. 3c, d), effectively competing with IC and facilitated by the presence of nearly isoenergetic excited triplet states (Fig. 3b). In contrast, benzil-type photoinitiators are excited to the S_2 state and lack efficient ISC pathways because no energetically proximate triplet states are available for either S_2 or S_1, resulting in dominant ultrafast IC in the sub-ps timescale and markedly reduced triplet-state formation (Fig. 3b, e) [85, 116, 118, 119]. When formed, the ensuing triplet states undergo α-cleavage on the ps timescale, thereby generating radicals for polymerization initiation.[116, 118] The kinetics of the α-cleavage for Me are nearly twice as slow as those observed for Bz and TMB, which is attributed to structural differences in the mesitoyl-radical precursors. A long-lived spectral component is assigned to absorption by the α-cleavage products for all three photoinitiators. Accordingly, the differences in early excited-state dynamics propagate directly into the efficiency of radical formation and, consequently, polymer-chain initiation [85].

The study by Wolf et al. [85] illustrates how fs TAS in combination with electronic-structure calculations serves as a powerful tool for mechanistic elucidation, enabling the identification of decisive design parameters for high-performance photoinitiators and providing a foundation for rational optimization of systems used in applications such as dental applications, biomaterials, 3D-printing and lithography [3, 85, 120–129]. Beyond photoinitiation, this approach is readily extendable to other photoinduced processes, including photocatalytic reactions, as a detailed understanding of the earliest photoinduced events could enable targeted control over reaction pathways and product selectivity. Nevertheless, the extent to which this experimental approach can deliver quantitatively predictive outcomes remains an open question, which the following case studies of selected photocatalytic systems will address, highlighting both the potential and the current limitations of fs-spectroscopic approaches in predictive reaction design.

3.3 CT-Mechanisms in Homogeneous Photocatalytic Systems Modulated by Intra- and Intermolecular Specifications

CT mechanisms that underpin photocatalysis—such as metal-to-ligand CT (MLCT), ligand-to-metal (LMCT), ligand-to-ligand CT (LLCT) or intramolecular CT (ICT)—are highly sensitive to intra- and intermolecular interactions, which modulate the photophysical properties and ultimately catalytic performance of the system [130–134]. As illustrated throughout the following case studies, the earliest photophysical events following photoexcitation critically determine reaction outcomes on much longer timescales. We further highlight the power of an approach combining electrochemical, theoretical, steady-state, and time-resolved spectroscopic techniques to enable a comprehensive

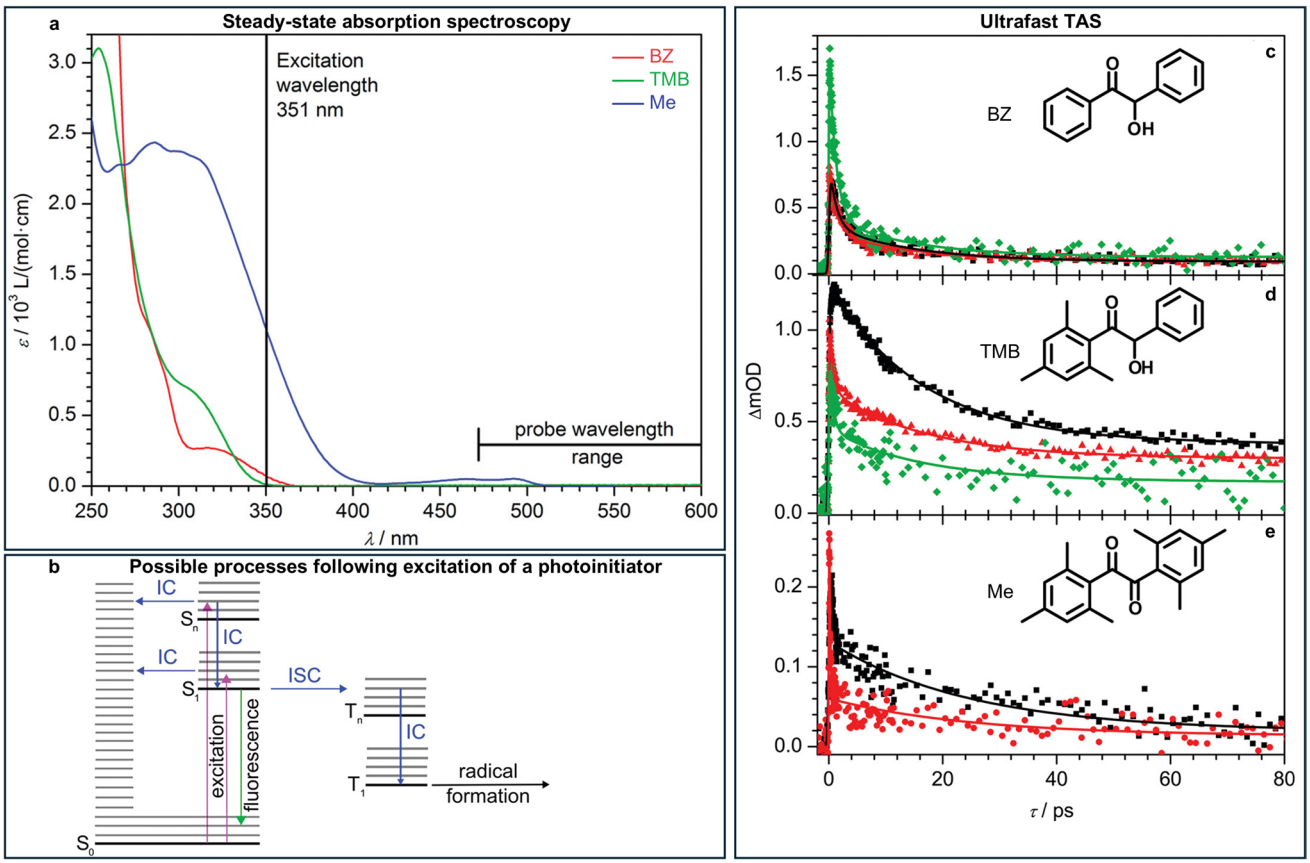

Fig. 3 **a** Wavelength-dependent extinction coefficients of Bz (red), TMB (green) and Me (blue). The different excitation coefficients at the excitation wavelength of the TAS the probe wavelength range are highlighted. **b** Accessible photophysical and -chemical pathways following excitation of a photoinitiator illustrated in a Jabłoński diagram. **c**–**e** TA spectra and fit functions of **c** Bz, **d** TMB and **e** Me in MeOH, excited at λ_{ex} = 351 nm and probed at λ_p = 470 nm (black), λ_p = 500 nm (red), λ_p = 600 nm (green).[85] Adapted with permission from Wolf et al. [85]. Copyright © 2012 American Chemical Society

mechanistic understanding of photocatalytic processes within complex environments.

Light-driven hydrogen evolution and homogeneous photocatalytic CO_2 reduction have traditionally relied on photosensitizers (PSs) and catalysts (Cats) based on costly scarce-metal architectures incorporating redox-active ligands [130, 135–151]. In response, significant efforts have been directed toward the development of photocatalytic systems based on earth-abundant elements [135, 137, 152–156]. Among these, heteroleptic Cu(I) complexes have emerged as particularly promising because they exhibit long-lived MLCT excited states and offer highly tunable redox and photoluminescence properties achievable through ligand design, outperforming their homoleptic analogues [135, 137, 157–163]. The closed-shell $3d^{10}$ configuration of Cu(I) precludes metal-centered (MC) d-d transitions associated with non-radiative deactivation [157, 164–166]; however, MLCT excitation often triggers a pseudo-Jahn–Teller (PJT) distortion, reducing the lifetime of the excited states [157, 164, 167, 168]. Moreover, the flattened geometry of Cu(I) complexes facilitates solvent coordination to the metal center, further quenching luminescence. To achieve long-lived excited states and mitigate these structural distortions, the use of rigid, sterically encumbered ligands is crucial [157, 164]. Systematic ligand design employing sterically demanding phosphines stabilizes the Cu(I) coordination environment and limits the extent of excited-state JT distortions, while bidentate diimine ligands further reinforce the coordination sphere, prevent the formation of homoleptic Cu-diimine complexes, and act as electron acceptors in photo(redox) processes [130, 135, 137, 157, 169–179]. Diimines are Schiff-base NN-chelating ligands that function as both σ-donors and π-acceptors, enabling decisive control over the electronic properties of the complex [130].

A particularly illustrative example is provided by a novel heteroleptic Cu(I) complex introduced by Bruschi et al. [130], featuring a non-innocent benzo[g]chinoxalin-2-one diimine ligand (BQXOT). This system combines PS and molecular photo-Cat functionality for direct CO_2 reduction within a single architecture, underscoring how deliberate ligand design can fundamentally shape photochemically reactivity. Upon photoexcitation, the PS mediates electron

transfer, while the Cat accepts these electrons to drive the catalytic reduction of CO_2 [130, 180–182]. Owing to the fully occupied d^{10} electron configuration of Cu(I), the lowest unoccupied molecular orbital (LUMO) is localized on the diimine ligand [130, 157], resulting in predominantly ligand-centered reduction processes and a lowest-energy absorption of MLCT character, in which electron density is promoted from a metal-based orbital into the first π^*-orbital of the ligand [130, 169, 183, 184]. Efficient photocatalytic CO_2 reduction under solar irradiation therefore requires precise tuning of the non-innocent ligand (NIL) to suitably lower the LUMO energy, thereby ensuring strong visible absorption and favorable electron transfer to catalytically active components. Steady-state absorption spectroscopy reveals intense ligand-centered ^{1}LC transitions in the UV region and a pronounced MLCT band in the visible, whose position and intensity depend on solvent environment (N,N-dimethylformamide (DMF) vs. dichloromethane (DCM)) (Fig. 4a). While the free ligand exhibits weak fluorescence, the complex is completely non-emissive in solution, indicating highly efficient non-radiative deactivation [130]. Electrochemical and spectroelectrochemical studies further revealed redox features indicative of potential electrocatalytic activity of the complex toward CO_2 reduction and demonstrated that the Cu(I) complex can accumulate up to three electrons on the BQXOT ligand [130, 149, 185]. Photocatalytic CO_2 conversion mediated by the Cu(I) complex was confirmed by reductive quenching of its excited state using a sacrificial electron donor, leading to selective formation of CO; no reaction occurred in the absence of light, donor or CO_2. Evidence of photoinduced CT processes involving the excited state of the complex was further provided by fs TAS using 400 nm excitation pulses. Upon photoexcitation, an intense ESA spanning the visible region was observed under N_2 atmosphere in both DCM and DMF (Fig. 4b). Global kinetic analysis revealed an initial sub-ps component attributed to ultrafast relaxation and structural reorganization (e.g. IC, flattening and JT distortion), followed by ISC on a sub-15 ps timescale to a triplet state whose lifetime is strongly solvent-dependent, ranging from several

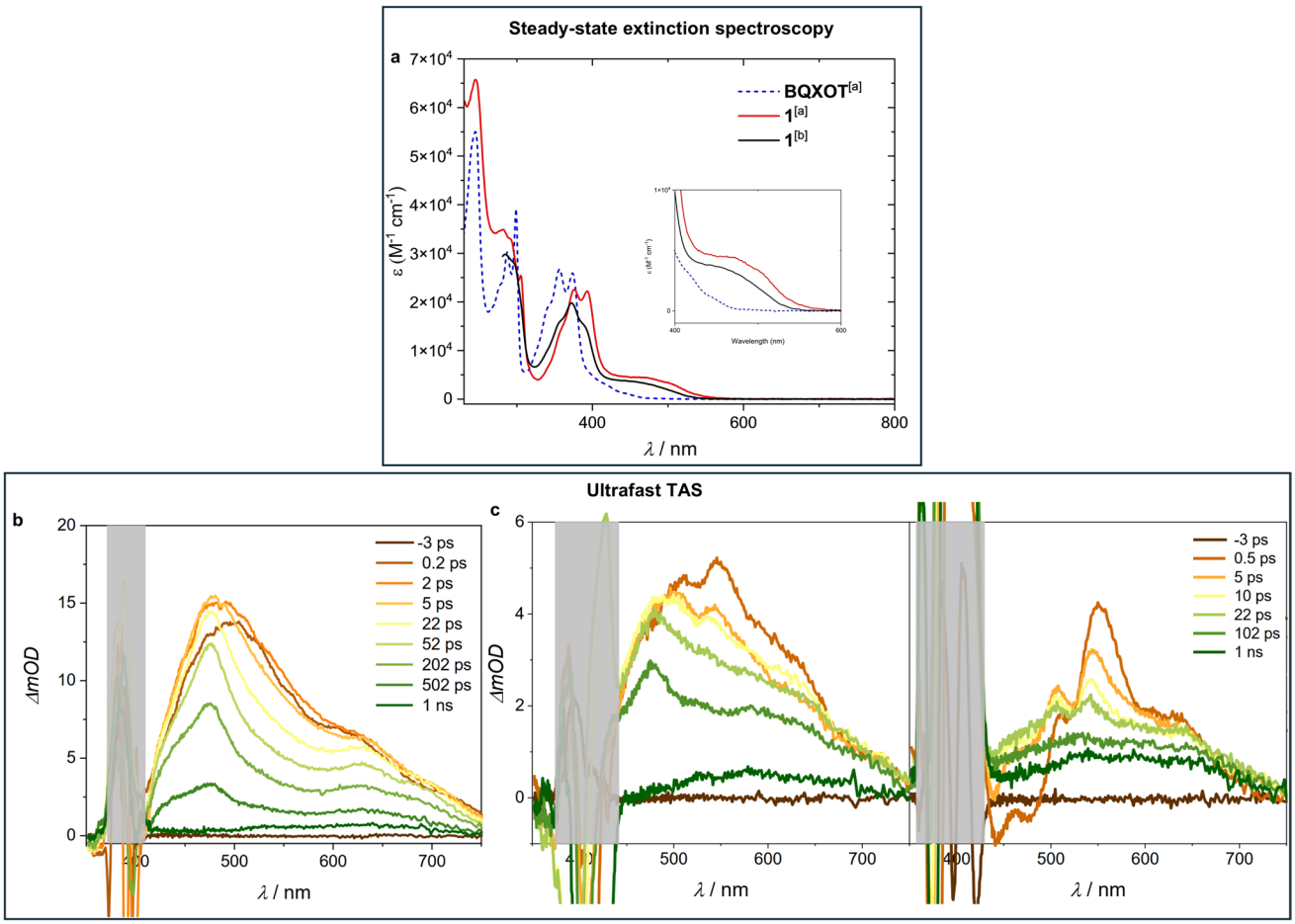

Fig. 4 **a** Wavelength-dependent molar extinction coefficients of BQXOT and the Cu(I) complex (1) in [a] DCM and [b] DMF. **b** TA spectra of 1 in DMF under N_2 atmosphere, λ_{ex} = 400 nm. **c** TA spectra of 1 in DMF in presence of BIH, recorded under N_2 atmosphere (1:20, left) and CO_2 atmosphere (1:100, right), λ_{ex} = 400 nm [130]. Adapted with permission from Bruschi et al. [130]. Copyright © 2024 The Authors. Chemistry—A European Journal published by Wiley–VCH GmbH

hundred ps in DMF to > 1 ns in DCM. In the presence of a sacrificial electron donor, fs-TAS captured rapid reductive quenching of the excited state within the first ps, accompanied by the appearance of new spectral features assigned to reduced ligand states (Fig. 4c), as well as shortened ISC and triplet lifetimes. Under CO_2 atmosphere, the early-time dynamics are markedly altered, including a faster ISC and extended triplet lifetime. By linking early-time excited-state dynamics to catalytic function, the authors demonstrated that CO_2 plays a decisive role in modulating the photoinduced reduction pathways and that the benzoquinoxalinone moiety facilitates the requisite charge build-up that enables CO_2 activation by acting as an electron reservoir. However, a comprehensive mechanistic understanding of the underlying photocatalytic process will require further investigation [130].

Photocatalytic water splitting imposes stringent demands on PSs and Cats due to its coupled multielectron chemistry. Beyond efficient photoinduced electron transfer, functional systems must temporarily store several redox equivalents while effectively suppressing competitive decay pathways, including charge recombination [149–151, 186]. A powerful strategy to address these challenges combines electrochemical pre-reduction with subsequent optical excitation, enabling controlled access to defined redox intermediates and direct interrogation of accumulative charge separation and storage by correlating spectroelectrochemical techniques with fs-TAS [149, 164]. Within this framework, Zhang et al. [149, 164] examined Cu(I) PSs comprising xanthphos in combination with either bidentate diimine or tetramethyl-substituted diimine ligands as prototypical systems for photoinduced two-electron accumulation (Fig. 5a–c). By integrating fs TAS, UV/Vis spectroelectrochemistry, resonance Raman spectroscopy and quantum-chemical calculations, the authors achieved a comprehensive assignment of the short-lived CT intermediates generated upon MLCT excitation and obtained detailed insights into the properties of their excited states relevant for two-photoelectron accumulation [149, 164]. Systematic variation of ligand substitution revealed that sterically demanding substituents proximal to the metal center are essential for stabilizing longer-lived excited states, whereas more distal electron-donating methyl groups exert only a marginal influence on the ultrafast dynamics (Fig. 5d) [149, 168, 187–190]. Most revealing were ultrafast TA spectroelectrochemistry experiments performed on singly reduced Cu(I) complexes. In contrast to their electrochemically unmodified counterparts, the MLCT excited states of the reduced PSs were found to be extremely short-lived, deactivating on a timescale of only a few tens of ps [149, 164, 168, 187, 188, 190–192]. This behavior was attributed to an ultrafast MLCT- to ILCT-IC localized on the reduced diimine ligand, which effectively precludes further photoinduced charge accumulation by limiting the lifetime of the excited, reduced PS [149, 164]. Thus, the potential for multielectron accumulation is governed not only by the energetic accessibility of suitable redox states or the HOMO–LUMO gap, but critically by the ultrafast dynamics determining the excited-state lifetimes of the reduced intermediates [149, 164, 188]. Accordingly, strategies such as fast reductive quenching by sacrificial electron donors or additional stabilization of reduced ligands through charge compensation by protonation may prove decisive for enabling efficient charge accumulation in photocatalytic systems [149, 151, 193–195].

The valence d electrons of first-row transition metals experience relatively weak ligand fields, which facilitates rapid population of low-lying MC states and thereby impedes the formation of long-lived MLCT excited states [155, 196–201]. When MC and MLCT states become energetically competitive, efficient non-radiative deactivation of MLCT states typically ensues [155, 202–206], yielding short-lived, non-emissive species unsuitable for photocatalysis [155,

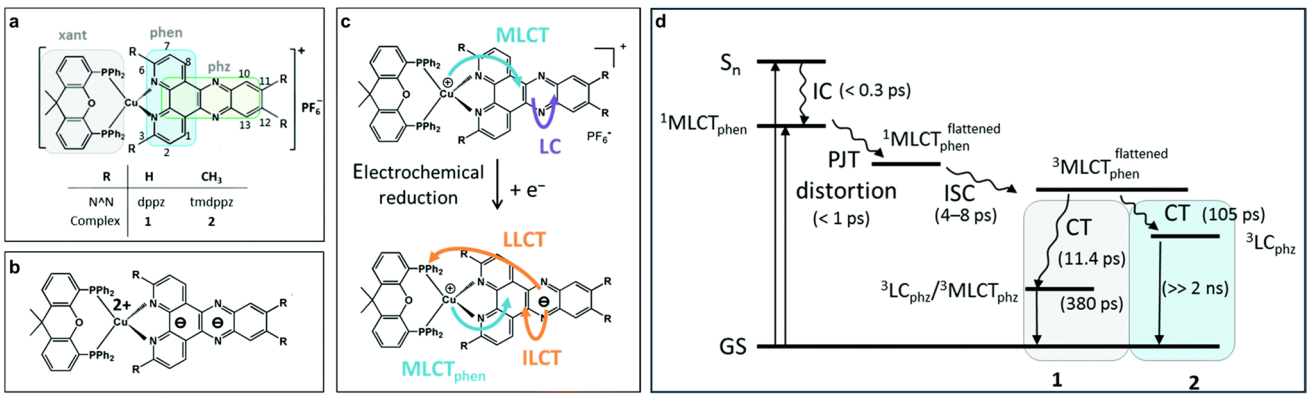

Fig. 5 **a** Molecular structures of Cu(I) complexes 1 and 2. **b** Intermediate formed by $MLCT_{phen}$ transition. **c** Overview of photoinduced CT pathways operative in 1 and 2 and their singly-reduced analogues. **d** Decay processes and time constants of 1 and 2 in ACN shown in a Jabłoński diagram [149]. Adapted with permission of the Royal Society of Chemistry, from Zhang et al. [149]; permission conveyed through Copyright Clearance Center, Inc

207, 208]. MC states typically undergo rapid non-radiative decay, via population of σ-antibonding d orbitals inducing structural distortions, low-energy surface crossings back to the ground state, and weakening metal–ligand bonds [206]; a common countermeasure is ligand-centered control of the MLCT/MC energy landscape. Building on earlier work from their group [209], Liu et al. [210] demonstrated that enhancing MLCT-frontier orbital delocalization with benzimidazolylidene-based ligands stabilizes the ^{3}MLCT state in a Fe(II) complex. As a consequence, the lowest-lying ^{3}MC is shifted above the ^{3}MLCT state, giving an unusually long ^{3}MLCT lifetime of 26 ps. A complementary, systematic approach was provided by Wegeberg et al. [155], who investigated isoelectronic, isostructural homoleptic tris(diisocyanide) complexes of the $3d^6$ metals Cr(0), Mn(I) and Fe (II). By tuning the effective nuclear charge, ligand-field strength and π conjugation of the ligand framework, the authors achieved fine control over the energetic ordering of ^{3}MLCT and ^{3}MC states. Moreover, the pyrene functionalization of the isocyanide scaffold enabled targeted control over intraligand excited states (IL_{Pyr}). TAS spanning the ultrafast regime to longer timescales, combined with complementary spectroscopic, electrochemical and theoretical methods, resolved the individual relaxation processes and provided a comprehensive picture of the energy levels and excited-state dynamics in these complexes (Fig. 6) [155, 211]. Distinct photophysical behavior emerged: the Cr complex exhibits long-lived ^{3}MLCT luminescence, the Mn analogue deactivates non-emissively via a lower-lying $^3IL_{Pyr}$ state, and the Fe complex undergoes rapid deactivation through a strongly distorted ^{3}MC manifold state that suppresses $^3IL_{Pyr}$ population. Because the lowest ^{3}MLCT state in Fe resides at comparatively high energy, a parallel $^1IL_{Pyr}$ fluorescence pathway becomes accessible alongside other deactivation channels. Overall, the study by Wegeberg et al. [155] illustrates that identical ligands paired with different $3d^6$ metal centers can generate fundamentally different photoactivities, underscoring the power of a rational metal–ligand design to tailor excited-state landscapes [155].

Light-driven Ni-catalyzed cross-coupling reactions have emerged as a versatile route to highly reactive intermediates [206, 212–214]. As discussed above, complexes of first-row transition metals often suffer from preferential population of rapidly deactivating, non-radiative MC d-d states, whereas sufficiently long-lived MLCT states are required to enable bimolecular electron-transfer processes [206, 215]. Within

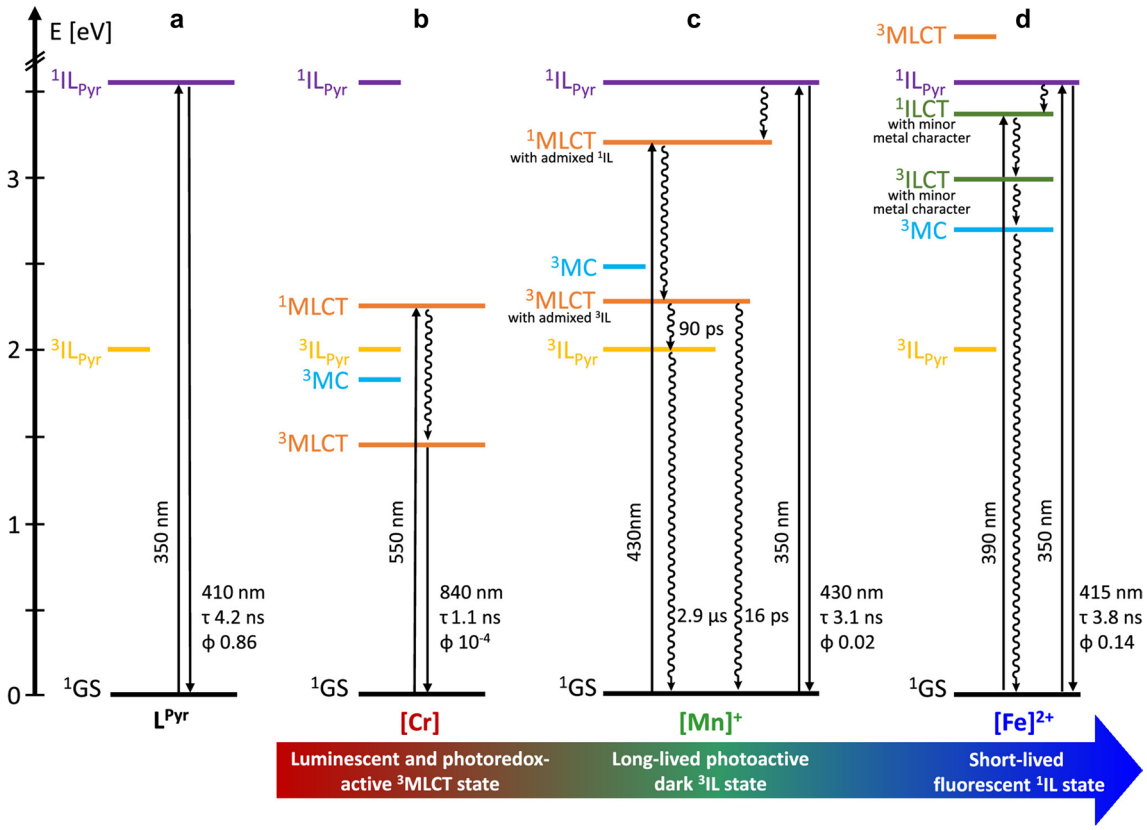

Fig. 6 Decay processes, time constants, luminescence quantum yields and luminescence wavelengths of **a** LPyr, **b** [Cr], **c** $[Mn]^+$ and **d** $[Fe].^{2+}$ illustrated in a Jabłoński diagram. Solid vertical lines: Radiative transitions, wavy vertical lines: non-radiative transitions [155]. Reproduced with permission from Wegeberg et al. [155]. Published by the American Chemical Society. This work is licensed under a Creative Commons Attribution 4.0 International License (CC BY 4.0)

this context, Ting et al. [206] examined the structure–reactivity-relationships of a series of Ni complexes bearing either bipyridine (bpy) or aryl ligands by combining ultrafast TAS with complementary spectroscopic methods and theoretical calculations. The TAS signatures on the earliest sub-ps timescales upon photoexcitation closely resemble the absorption features of the bpy radical anion, indicating an initially populated MLCT state that formally reduces the bpy ligand. Within a few ps, this MLCT state evolves into a longer-lived excited state of d-d character, as supported by DFT calculations. Remarkably, the lifetime of this long-lived excited state remains essentially invariant across systematic substitution of both ligand fragments with electron-donating and – withdrawing groups—[206] a behavior inconsistent with MLCT assignment [206, 215, 216]. Instead, the authors propose that the ^{3}d-d excited state, characterized by weakened Ni(II)-aryl bonds, promotes photoinduced homolytic bond cleavage, generating aryl radicals alongside catalytically active Ni(I) species [206].

Bis(dipyrrinato) Zn(II) complexes are intramolecular donor–acceptor systems whose CT dynamics are highly sensitive to ligand design and solvent polarity [131, 217–220]. Despite the d^{10} electron configuration and the concomitant redox inertness of the Zn(II) center, coordination of two dipyrrin ligands enables ICT that can evolve into non-emissive charge-separated (CS) states [131, 221–224]. These CS states may recombine to long-lived triplet states, a feature central to photocatalysis [131, 219, 221, 225–227]. While ground-state symmetry breaking—achieved, e.g. through heteroleptic complex formation or tailored ligand design—can suppress CS state population, homoleptic Zn-dipyrrin complexes permit a solvent-dependent, photoinduced ICT driven by excited-state symmetry breaking, which is stabilized in polar media [131, 219–221, 228–232]. Leier et al. [131] showed that ligand structure, substitution patterns (Fig. 7a) and environment govern the excited-state dynamics of these homoleptic Zn(II) dipyrrin complexes and their photocatalytic oxidation performance by correlating fs-ns TA spectra and steady-state data [131]. Coordination to Zn induces strong intramolecular CT character; increasing solvent polarity significantly reduced extinction coefficients (Fig. 7b, c) [131, 217, 223, 228, 233, 234], while stabilizing a non-emissive CS state at the expense of fluorescence quantum yield and lifetime [131, 219, 223, 228]. Emission spectra display substantial Stokes shifts exceeding 450 cm^{-1}, indicative of excited-state relaxation prior to emission, attributable to conformational, vibrational or electronic reorganization [131, 217, 218, 233, 235]. Functional substituents can modestly increase fluorescence quantum yields by restraining structural distortions. Supported by theoretical calculations, a thermally activated conversion from the emissive $^1(\pi - \pi^*)$ excited state (D-Zn-D*) to a non-emissive CS state (D^+-Zn-D^-) involving ICT was proposed [131, 217]. Time-resolved studies (Fig. 7c–g) show that free ligands relax within appr. 100 ps, whereas Zn complexes exhibit long-lived transients into the ns regime, indicating coupled singlet–triplet dynamics [131, 227]. Ultrafast processes on the 100 fs timescale, enhanced in polar solvents, correlate with reduced fluorescence quantum yields and provide compelling evidence for CT-state formation. The photophysical behavior dictates photocatalytic pathways: Zn-dipyrrins can promote electron-transfer oxidation (generating superoxide via reduction of O_2 by the photo-Cat radical anion) or energy-transfer oxidation (producing singlet O_2 through triplet–triplet annihilation) (Fig. 7h). Early CT and triplet dynamics resolved by fs-ns TA determine which ROS-generation route dominates, with ICT-state formation being a key determinant for electron-transfer-driven catalysis.[131] Alqahtani et al. [221] employed TAS to quantify triplet-state formation in Zn-dipyrrins with and without heavy-atom substitution across different solvent. In absence of heavy atoms, the triplet yield strongly dependent on polarity, whereas incorporation of heavy atoms renders the triplet population largely insensitive to the surrounding medium, indicating distinct ISC mechanisms that must be understood to design chromophores with high triplet quantum yields [221].

Al, the most abundant metal in the earth's crust, is an attractive platform for replacing transition metals in catalysis, but its non-noble character limits access to d-block reactivity. As a result, strategies that mimic transition-metal behavior with Al—particularly redox cycles based on a main group element—have gained increasing prominence [132, 236–242]. Photochemical homolysis via LMCT or LLCT normally demands high-energy UV excitation because Al complexes possess high-lying acceptor orbitals and unfavorable energetics associated for accessing sub-valent Al species [132, 243–246]; incorporation of redox-active NILs introduces low-lying acceptor orbitals and enables LLCT under significantly milder, visible-light conditions [132, 236, 247]. Wenzel et al. [132] demonstrated this concept with Al(III) complexes bearing tridentate, monoanionic bis(pyridylimino)isoindolide-(BPI)-ligands (Fig. 8a) that undergo visible-light-induced Al–C bond homolysis. By combining steady-state and transient UV/Vis spectroscopy, spin- and radical-trapping experiments, EPR/NMR and quantum-chemical calculations, they mapped a radical-polar-crossover mechanism, in which the BPI scaffold provides low-lying orbitals for LLCT. Systematic BPI substitution tuned solubility and shifted ligand-centered transitions bathochromically into the visible region (Fig. 8b, c). TD-DFT shows the lowest-energy S_1 excitation (~452 nm) to be strong LLCT, transferring electron density from Al–C σ-bonds into π^*-orbitals of the BPI ligand [132].

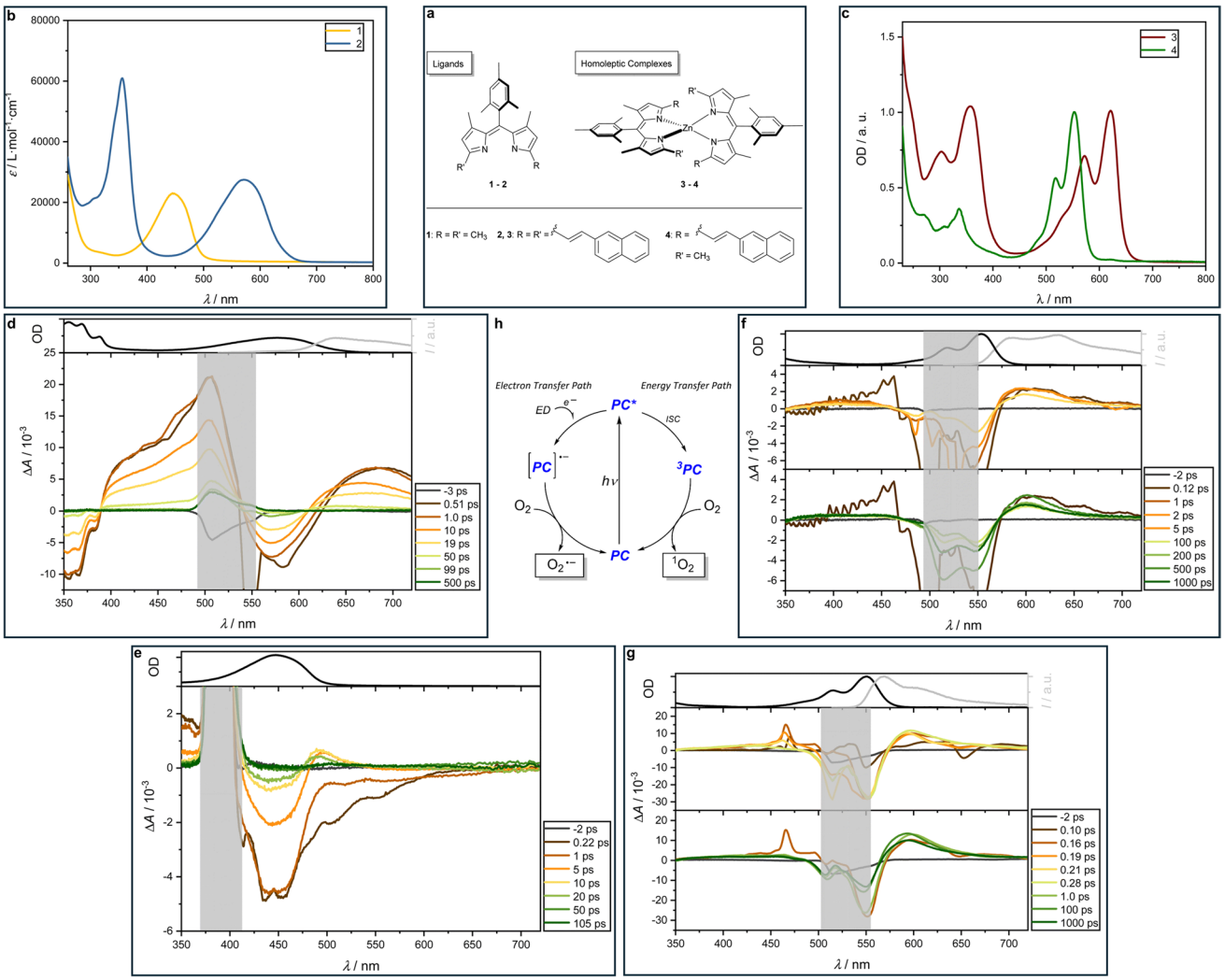

Fig. 7 **a** Structure of ligands 1–2 and zinc complexes 3–4. **b** Wavelength-dependent molar extinction coefficients of ligands 1 (yellow) and 2 (blue) in DCM. **c** Normalized absorption spectra of 3 (red) and 4 (green) in DCM. **d**–**g** TAS of (d) 2 in DCM λ_{ex} = 575 nm, **e** 1 in DCM λ_{ex} = 400 nm, **f** 4 in DCM λ_{ex} = 550 nm, **g** 4 in EtOH λ_{ex} = 560 nm at indicated delay times. Areas influenced by scattering effects from the pump pulse are masked by the grey box. Top section: Normalized steady-state absorption (black) and emission (grey) spectra. **h** Schematic of potential ROS formation pathways from a photo Cat (PC): Electron transfer involves a donor (ED) reducing the PC to produce superoxide, energy transfer proceeds via ISC to the triplet state of PC, enabling singlet oxygen generation though triplet–triplet annihilation [131]. Adapted from Leier et al. [131]. Published by the Royal Society of Chemistry. This article is licensed under a Creative Commons Attribution 3.0 Unported Licence (CC BY 3.0)

The associated vibronic progression reflects skeletal BPI vibrations [132, 248, 249]. Barrierless S_1 relaxation leads to homolytic Al–C cleavage, affording a reduced BPI-Al radical that, without efficient trapping, undergoes ligand alkylation; [132, 250] this photo-induced pathway contrasts with thermally driven alkylation in NIL-organo-Al systems [251–254]. fs-ns TAS with 340 and 400 nm excitation revealed an immediate broad ESA across the visible region and a weak SE component hidden by the very low fluorescence quantum yields of both free ligand and Al complex (Fig. 8d, e). The ESA rises within the 100 fs instrument response, indicating vertical excitation to a hot Franck–Condon singlet state followed by sub-ps structural reorganisation; [21, 132, 255] nearly identical transient spectra for 340 ($S_2 \leftarrow S_0$) and 400 nm ($S_1 \leftarrow S_0$) excitation imply ultrafast IC between singlet excited states.

For the free ligand (1-H) the ESA decays within appr. 50 ps, with a transient SE band on a few-hundred-fs timescale, consistent with rapid IC via a conical intersection. In contrast, the Al complex (1-$AlMe_2$) shows ESA persisting > 1 ns, reflecting slowed ground-state repopulation. Global kinetic analysis identified a common sub-ps IC component and two slower (tens–hundreds ps) components exclusive to the Al complex, representing branching into distinct relaxation pathways; amplitude analysis indicated

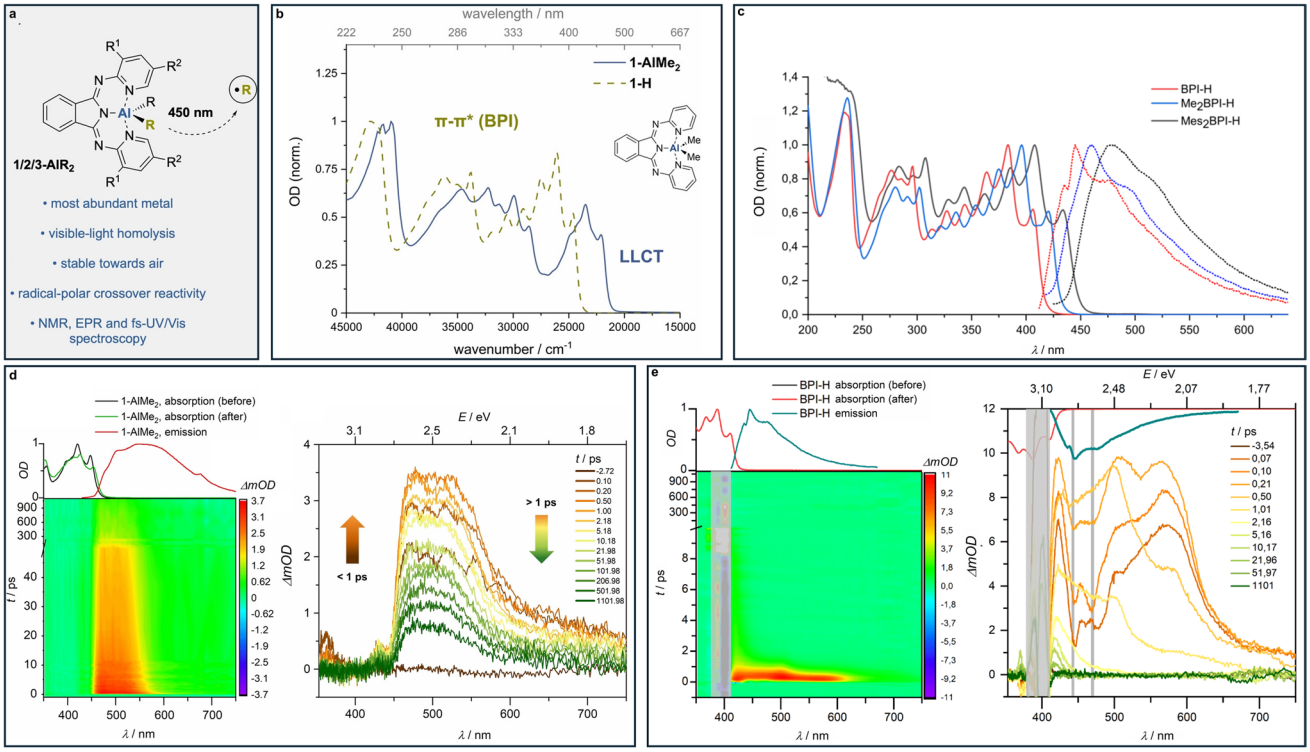

Fig. 8 **a** Designed CT homolysis. **b** Normalized stationary absorption spectra of 1-H and 1-AlMe$_2$ in n-hexane. **c** Normalized stationary absorption (straight lines) and emission spectra (dotted lines) of 1-H (red), 2-H (blue) and 3-H (grey). **d**, **e** Contour diagram (right) and TAS (left) in benzene of **d** 1-AlMe$_2$ λ_{ex} = 340 nm and **e** 1-H λ_{ex} = 400 nm at indicated delay times. Top section: Normalized steady-state absorption spectra before (VT) and after (NT) transient measurements and emission spectra. Superimposed fluorescence is marked by grey bars and inversed stationary absorption (red) and fluorescence spectra (green). Adapted from Wenzel et al. [132]. Published by Wiley–VCH GmbH. This work is licensed under a Creative Commons Attribution 4.0 International License (CC BY 4.0)

that ~ 20% of the excited population follows the photochemical route that yields ultrafast Al–C homolysis.

Thus, irradiation of 1-AlMe$_2$ at 340 nm or 400 nm populates S_1, from which the molecule either relaxes non-radiatively or undergoes a dissociative vibrational motion that efficiently cleaves the Al–C bond, generating a methyl radical and a masked Al(II) radical (1-AlMe*). The polarity of the Al–C bond and the efficiency of vibrational energy transfer are the key determinants governing photo-reductive CT homolysis in main-group systems [132].

Thermally activated delayed fluorescence (TADF) has emerged as a key design principle for photocatalytically active chromophores, as it enables access to long-lived excited states that are crucial for bimolecular photochemical processes [134, 256]. Central to this mechanism is a small energy gap between the lowest S and T excited states, which allows thermally activated rISC [134, 257, 258]. Zhang et al. [134] compellingly demonstrated this concept using a Zr(IV)-based early transition-metal complex featuring a d^0 electron configuration and excited states with pronounced LMCT character. Because d^0 systems lack low-lying MC states, rapid non-radiative deactivation is avoided. Pairing the electron-deficient Zr center with strongly electron-rich pyridine-pyrrolide or pyridine-dipyrrolide (PDP) ligands inverts the usual MLCT pathway to a LMCT-dominated excitation, yielding long-lived photoluminescence from states with substantial LMCT character and efficient photoredox-active excited states [134, 259–262]. Visible absorption bands were assigned to mixed ^{1}IL/^{1}LMCT transitions by TD-DFT. The lack of solvatochromism across solvents of varying polarity indicated that photoexcitation is not accompanied by a significant change in the molecular dipole moment. Emission is independent of excitation wavelength and solvent polarity, mirroring the lowest-energy absorption band. Temperature-dependent emission shows a gradual intensity decrease on cooling, accompanied by the emergence of a second, closely spaced component that dominates at low temperature. This behavior reflects emission from S_1 (fluorescence) and T_1 (phosphorescence); at low temperature phosphorescence dominates, while increasing temperature activates rISC, making delayed fluorescence the main pathway. The near-identical fluorescence and phosphorescence spectra imply comparable mixed IL/LMCT character for both states, in agreement with DFT. Temperature-dependent lifetime measurements further corroborate the TADF mechanism, revealing a decrease in emission lifetime with

increasing temperature that can be described by a kinetic model involving two emissive states in rapid thermal equilibrium. The absence of prompt fluorescence and the strictly monoexponential decay observed over the entire temperature range indicate highly efficient ISC and near-complete depopulation of the initially populated S_1 state. Ultrafast TAS at RT (Fig. 9a, b) supports a consistent kinetic scheme (Fig. 9c): photoexcitation initially populates a S_1 state with a mixed ^{1}IL/^{1}LMCT character, which undergoes IC within appr. 1 ps, plausibly driven by subtle JT-type distortion. ISC follows on an appr. 12 ps timescale to a long-lived T_1 state with ^{3}IL/^{3}LMCT character that persists through the fs TAS observation window. Complementary µs-TAS measurements confirm the assignment of this state to a T_1 state and agree with lifetimes obtained from time-resolved emission spectroscopy. Combining these data with the S_1-T_1 energy gap yields an rISC time constant of appr. 41 ns at RT. Cyclic voltammetry further reveals reversible oxidative redox processes while preserving single-electron reduction chemistry (Fig. 9d). Together with the exceptionally long excited-state lifetimes, this redox accessibility renders Zr-based LMCT sensitizers ideally suited for photoinduced bimolecular reactions under diffusion-controlled conditions—an essential requirement for applications in photoredox catalysis and solar fuel chemistry. Looking ahead, a central challenge will be the rational control of TADF lifetimes, which will be critical for tailoring PSs to specific catalytic and energy-conversion applications [134].

In photoredox catalysis, including arylation reactions, metal-free organic Cats have emerged as powerful alternatives to metal-based systems [263–266] and substituent effects are known to exert a decisive influence on the excited-state dynamics of these organic donor–acceptor architectures [224, 266, 267]. Aryl chlorides represent particularly challenging substrates for photoredox catalysis due to the high strength of the C(sp^2)-Cl bond and their strongly negative reduction potentials [266]. Building on earlier work [268–272], Weick et al. [266] demonstrated that highly electron-rich N-phenylphenothiazines enable direct activation of aryl chlorides via photoinduced electron transfer, obviating the need for electrochemical activation [273, 274] or more elaborate photoredox strategies [275–278]. By systematic substitution at the phenyl moiety of the phenothiazines, excited-state reduction potentials as negative as appr. -3.0 V were achieved, thereby rendering aryl chlorides bearing both electron-withdrawing and electron-donating substituents amenable to activation. This strategy was exemplified in photocatalytic borylation and phosphonylation reactions. Strikingly, Cats that are closely related in structure displayed pronounced differences on catalytic efficiency. Decisive mechanistic insight into these performance differences was obtained through the combined application of fs TAS and spectroelectrochemical investigations under oxidative conditions [266]. Whereas the excited singlet and triplet states of the neutral phenothiazines exhibit largely similar photophysical characteristics [266, 279], their corresponding radical cations display markedly divergent excited-state dynamics. In the case of dialkylamino-substituted phenothiazines, a second photoexcitation of the radical cation induces transfer of the positive charge to the phenyl substituent [266]. This process is accompanied by substantial structural reorganization [266, 280–282], which extends the lifetime of the excited radical cation into the ns regime. The enhanced photocatalytic activity of these systems is attributed to the resulting suppression of rapid electron back transfer.[266, 279] Cats in which this structural and electronic reorganization is inhibited by steric or conformational constraints exhibit diminished reactivity [266].

Taken together, the studies discussed in this section exemplify how ultrafast spectroscopic approaches in concert with complementary techniques extend well beyond excited-state characterization, providing essential insight into structure-dynamics-reactivity relationships and guiding the rational design of molecular architectures with tailored excited-state properties for several applications, including photocatalysis.

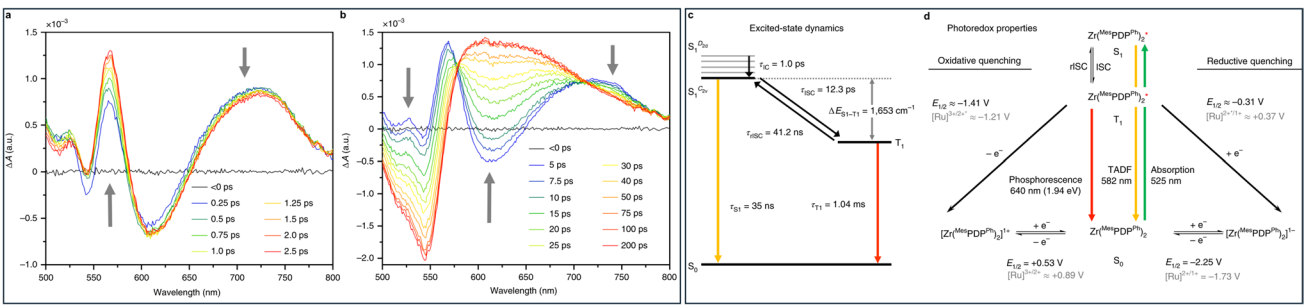

Fig. 9 **a**, **b** TAS of Zr(^{Mes}PDP^{Ph})$_2$ λ_{ex} = 480 nm at indicated delay times. **c** Excited state dynamics of TADF with parameters obtained from temperature-dependent emission and transient absorption. We interpret the slanted arrows as representing the superposition of at least two processes, such as IVR/VR and ISC. **d** Excited state photoredox properties. [134] Adapted from Zhang et al. [134] with permission from Springer Nature

4 Perspective

4.1 The Red-Edge Effect in Photochemistry

First identified in fluorescence spectroscopy, selective excitation of a fluorophore at the long-wavelength edge of its absorption band can, under suitable conditions, induce systematic red-shifts in emission spectra as well as extended excited-state lifetimes [34, 36, 37]. This excitation wavelength-dependent emission behavior is generally consistent with Kasha's rule [79] and Vavilov's law [283], provided that the ensemble of excited molecules is energetically heterogeneous due to distinct interactions of individual fluorophores with their local environment [22, 32, 34, 284]. Beyond non-specific solvent effects, such as those arising from solvent polarity or viscosity, specific interactions between solvent and fluorophore, e.g. hydrogen bonding, can exert a significant influence [28, 285–287]. When excitation is selectively shifted to the red edge of the absorption spectrum, the energy is insufficient to excite the entire ensemble. Instead, species whose excited states are stabilized by strong environmental coupling are preferentially excited, resulting in red-shifted emission [32–35]. This so-called red-edge excitation is intimately linked to slow dielectric relaxation of the surrounding medium, which prevents complete equilibration of the excited state during its lifetime [22, 33, 34, 36, 284]. The principle of excitation wavelength-dependent selectively manifests in numerous apparently counterintuitive photochemical observations, including non-monotonic action plots, excitation-dependent quantum yields and deviations from peak absorption-based reactivity assumptions [38–56]. These observations suggest that red-shifted excitation can selectively access alternative reaction pathways. For instance, Marschner et al. [288] demonstrated that wavelength-dependent photocycloadditions exhibit a non-linear relationship between reactivity and absorption intensity. Their action plots and solvent comparisons highlight how environmental factors modulate quantum yields, reinforcing the concept of excitation wavelength-dependent reactivity central to the red-edge effect. Further, Fast et al. [57] examined oxime ester photoinitiators and found that maximum conversion occurred at higher wavelengths compared to the maximum absorption peak with low molar extinction coefficients (Fig. 10a, b). This counterintuitive result supports the idea that absorption spectra alone are insufficient predictors of photochemical efficiency [48, 57]. Kanchana et al. [48] interpreted the results on their studies on oxime esters in terms of wavelength-dependent balance between singlet and triplet cleavage, where longer-wavelength excitation favors triplet formation and enhanced radical diffusion. Kalayci et al. [40] recorded persistent [2+2] cycloaddition reactivity of acrylamidopyrene at 490 nm, well beyond the absorption maximum at 370 nm and Kim et al. [289] observed red-shifted maximal efficiency in the ring contraction of N-aryl-azacycles. Although the mechanistic origins of these discrepancies between absorption strength and photochemical reactivity remain not completely understood [43, 290], the evidence collectively points to the interplay of multiple photophysical and -chemical processes, with system-specific relative contributions [22, 43]. One contributing factor is supposed to be the microenvironment surrounding the molecules. Carroll et al. [26] attributed wavelength-selective reactivity in a pyrene-chalcone system in [2+2] cycloadditions to selective excitation of specific microenvironments, modulating accessible molecular transitions and altering product distributions depending on irradiation wavelength (Fig. 10c). Furthermore, the four fundamental pillars of precision photochemistry–molar extinction, wavelength-dependent quantum yield, concentration of the chromophores and duration of irradiation–were outlined by Pashley-Johnson et al. [54]. These parameters are intrinsically interconnected and collectively define the experimental conditions to be employed, including the irradiation wavelength, light intensity and solvent environment [54].

Taken together, these studies indicate that wavelength- and environment-dependent reactivity represents a general photophysical principle, likely extendable to other photochemical reactions, e.g. photocatalytic processes. A deeper mechanistic understanding requires direct access to ultrafast dynamics that govern branching among competing relaxation pathways, ultimately determining reaction yields, alongside a systematic investigation of their dependence on key reaction parameters [22, 28, 43]. Solvation dynamics play a central role, as solvent–solute interactions influence both the energetic landscape of electronic states and their transitions, as well as the structural evolution of photoexcited molecules [28]. Using fs TAS, Strolka et al. [27] demonstrated that ISC times in bengal rose can be continuously tuned by varying the solvent composition, showing that when electronic transitions occur faster than solvent reorganization, they can dominate photochemical outcomes. Venkatraman et al. [28] similarly illustrated, using selected model compounds including photoredox Cats, how solvent interactions can steer photochemical pathway selectivity. Studies by Kimura [291], Suda [292, 293] and Fukuda et al. [294]. on excitation wavelength-dependent excited-state intramolecular proton transfer (ESIPT) dynamics in flavonoids across conventional solvents and room-temperature ionic liquids (RITLs) underscore the critical role of early solvation processes in directing photochemical reactions. Due to extremely slow solvent relaxation in RITLs compared to conventional solvents, competing processes can be observed on markedly longer timescales. Both the rate and yield of tautomerization decreased with increasing excitation

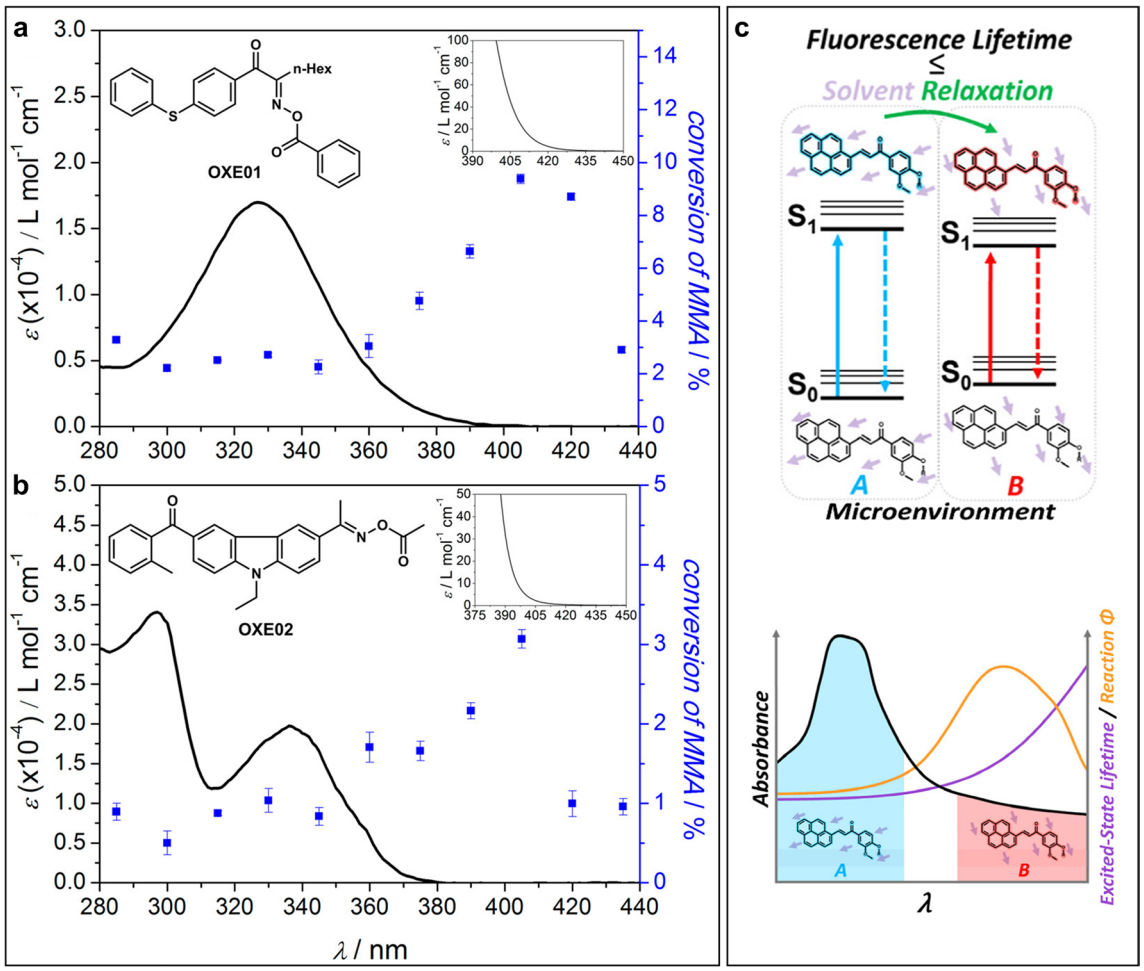

Fig. 10 **a**, **b** Steady-state absorption spectra and wavelength-dependent methyl methacrylate conversion for **a** OXE01 and **b** OXE02 under constant photon exposure (60 μmol per irradiation wavelength, PLP synthesized) [57]. Adapted with permission from Fast et al. [57]. Copyright 2017 American Chemical Society. **c** Top: Simplified Jabłoński diagram of the ground and excited states for a chromophore under the influence of different microenvironments A and B. Bottom: Dependence of absorbance, excited-state lifetime and reaction quantum yield on microenvironments A and B [26]. Adapted with permission from Carroll et al. [26]. Copyright 2025 American Chemical Society

wavelength in RITLs and the highly viscous solvent glycerin triacetate, indicating that ESIPT competes with solvent relaxation under these conditions [22, 291–294]. The concept of precision photochemistry has also been adopted in photoredox catalysis [54, 295]. Reeves et al. [296] showed that the efficiency of a reversible addition-fragmentation chain-transfer (RAFT) photopolymerization is maximized at wavelengths that do not correspond to either the monomer or photo Cat absorption maxima. Ghosh et al. [297] exploited light-color-controlled generation of distinct redox states of rhodamine 6G for chromoselective C-H arylation, establishing a direct link between excitation wavelength, redox potential and selectively in catalytic systems. When radical chain reactions compete with photocatalytic pathways, the quantum yield of photoredox catalysis depends not only on excitation wavelength but also on light intensity [54, 298, 299]. Kerzig et al. [300] demonstrated that controlled variation of photon flux in an iridium photo Cat enables selective switching between triplet energy transfer and electron transfer processes as one—and two photon mechanisms, thereby precisely tuning the available redox potential for challenging reductions. Selective excitation at the red edge of the absorption band is also of particular relevance for biological systems, as it may enable excitation of chromophores whose principal absorption bands lie in the UV region using visible light, which is considerably more benign for biological applications [50, 301, 302]. Collectively, these studies highlight that red-shifted reactivity is not a marginal phenomenon but a fundamental design principle. Consequently, a refined understanding of wavelength-dependent reactivity and its modulation by external factors is essential for the targeted control of photochemical and photocatalytic processes through precisely tuned photonic fields [288].

4.2 Mechanistic Insights and Design Principles

The rational design of tailor-made photoactive systems requires a detailed understanding of excited-state dynamics across multiple timescales. Only by integrating ultrafast spectroscopic techniques, quantum-chemical modeling and long-timescale observations, excited-state lifetimes and branching ratios can be accurately characterized. These insights provide the foundation for constructing solvent-dependent reactivity maps and for establishing concrete guidelines in the selection of appropriate ligands and solvation environments. Such mechanistic understanding underpins the rational development of photoactive systems with tailored properties, including selective reactivity and enhanced quantum yields. The validity of these design strategies is exemplified by several case studies.

Mauri et al. [303] provided a mechanistic framework for radical formation via two- and three-photon excitation in 3D laser nanoprinting. The efficiency and resolution of this process are critically governed by the performance of the photoinitiators employed [304, 305], which in turn depends on the underlying radical generation pathways, the reactivity of the produced species and the absorption characteristics of the molecules. A pivotal factor in radical generation is ISC between singlet and triplet states, which competes with IC and radiative relaxation. Accordingly, both efficient ISC and sufficiently long-lived triplet states are prerequisites for effective initiation [303, 306]. However, the photochemical performance of common photoinitiators cannot be inferred solely from their chemical composition or the electronic structure in the ground or lowest triplet state. Quantum mechanical analyses of 7-diethylamino-3-thenoylcoumarin (DETC) photoinitiators reveal how triplet state dynamics and hydrogen atom transfer reactions critically govern polymerization efficiency, providing direct guidance for the design of systems with tailored excited-state lifetimes and reactivity [303]. A complementary perspective was presented by Wolf et al. [3], who evaluated the suitability of organic photoinitiators for Stimulated-Emission-Depletion (STED) -inspired far-field lithography. Using fs pump-probe spectroscopy, they directly monitored the excited-state dynamics of DETC and isopropylthioxanthon (ITX) in solution, capturing the competition between SE and ESA. While STED-based approaches rely on efficient depletion of the first excited singlet state via SE induced by a second laser, competing ESA accesses higher-lying states with poorly controllable dynamics and potentially undesired side reactions, thereby impacting both photoinitiator transition properties and polymerization dynamics (Fig. 11a) [3]. Efficient STED-inspired lithography therefore requires dominant SE coupled with minimal ESA [3, 307]. Experimental results confirmed SE dominance over ESA for DETC, in contrast to ITX (Fig. 11b–d). Global analysis of transient responses, including amplitude ratios of SE and ESA as well as extracted time constants, and further transient anisotropy data corroborate this finding. For DETC, pronounced SE at 532 nm with a decay time of appr. 100 ps was observed, rendering this photoinitiator particularly suited for pulsed depletion strategies in direct STED laser writing, whereas ITX does not meet these criteria. This study emphasizes that the relative balance of competing processes such as SE and ESA constitutes a critical design parameter for functional photoinitiators, accessible only via ultrafast time-resolved methods [3].

Thielemann et al. [308] further demonstrated in acetylacetonate-ligated lanthanoid complexes that the ligand environment can selectively modulate photodynamics. fs TAS revealed pronounced ligand-specific behavior, with relaxation times sensitive to the identity of the lanthanoid center, indicative of intramolecular energy transfer from ligand to metal. Knöfel et al. [309] additionally showed that coordinating different metal fragments to a homoleptic dimolybdenum metalloligand allows fine-tuning of optical properties directly correlated with fluorescence quantum yields. Taken together, these studies underscore that a systematic characterization of how excited-state landscapes and lifetimes are modulated by intra- and intermolecular interactions is essential for the rational tailoring of photoactive systems. Such mechanistic insight is indispensable for achieving targeted functionalities with maximal efficiency in advanced photochemical applications.

5 Conclusion

Femtosecond broadband absorption spectroscopy provides a powerful lens into the elementary mechanisms of photoexcited molecules in complex environments. As highlighted throughout the case studies presented in this review, the reactivity, selectivity and overall efficiency of photochemical systems are determined to a remarkable extent by the earliest ultrafast events following photoexcitation. A rigorous mechanistic understanding of these primary steps provides the foundation for the deliberate modulation of photophysical properties and ultimately for the rational design of functional light-responsive materials. Since the seminal contributions of Ahmed H. Zewail [15, 16, 23–25], ultrafast spectroscopy has undergone a transformative evolution over the past two to three decades. Continuous advances in laser technology and detection methodologies have progressively enhanced both temporal and spectral resolution, enabling an increasingly sophisticated dissection of competing elementary pathways and their interplay [11–14, 16, 17, 310, 311]. Given the current pace of innovation, further conceptual and

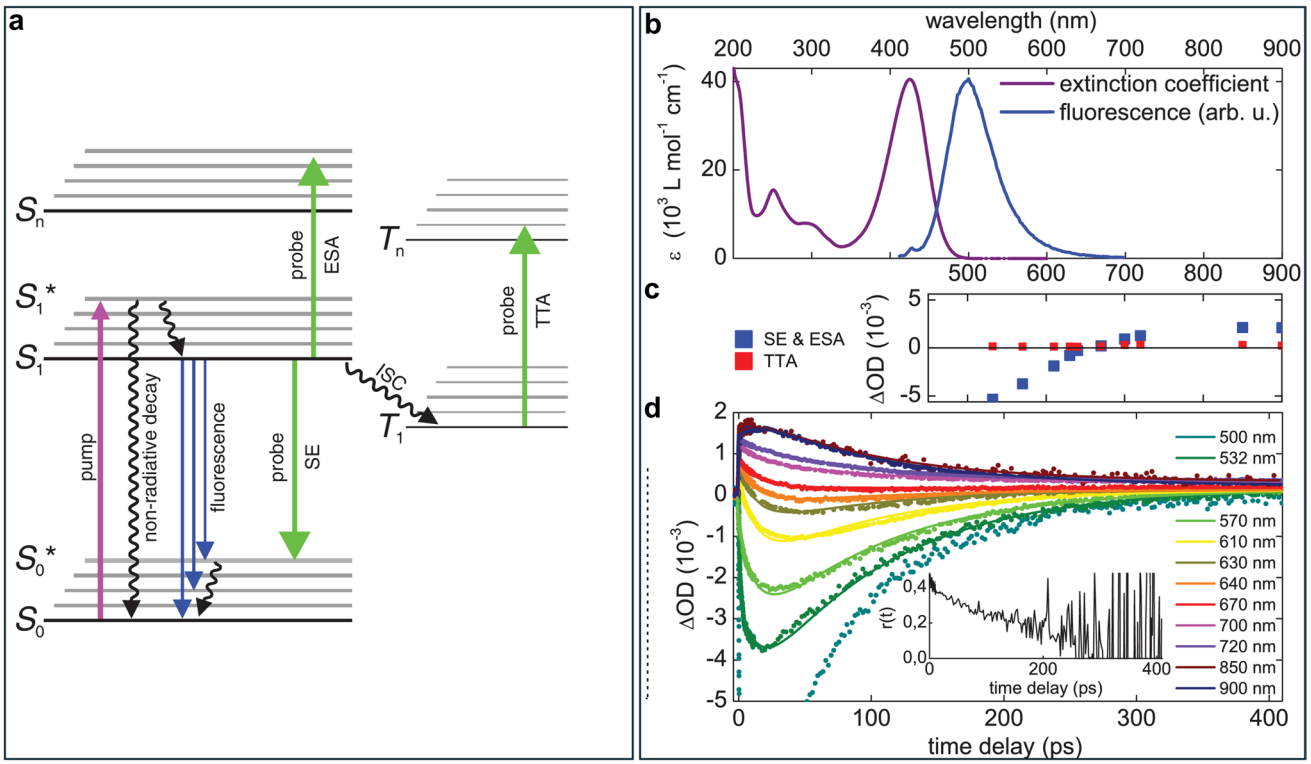

Fig. 11 **a** Proposed photoinitiator transitions for STED-inspired optical lithography, depicted in a Jabłoński diagram. **b** Molar excitinction coefficient and emission profile of DETC in EtOH. **c** Extracted fit coefficients for the combined SE + ESA and TTA contributions. **d** Pump-probe absorption spectroscopy of DETC in EtOH at selected probe wavelengths following excitation λ_{ex} = 387.5 nm. Solid lines result from a global analysis of the transient data [3]. Adapted with permission from Wolf et al. [3] © Optical Society of America

technical breakthroughs are not only expected but likely to redefine our understanding of photoinduced reactivity in the near future. In this review, we have provided an integrative perspective on central concepts in contemporary photochemistry that have emerged from ultrafast studies. Strategies such as the targeted manipulation of CT states, the mechanistic elucidation of solvent-controlled dynamics and the exploitation of excitation-wavelength-dependent reactivity extend far beyond molecular model systems and offer substantial opportunities for transition into photocatalysis. As discussed, emerging examples already demonstrated that these principles can be successfully implemented in catalytic contexts. The synergistic integration of ultrafast spectroscopy with steady-state characterization and advanced theoretical approaches will be crucial achieving predictive control over photocatalytic transformations and for establishing new design paradigms in light-driven chemistry.

Acknowledgements We acknowledge continued key support from the Karlsruhe Institute of Technology (KIT). We are very grateful to Prof. Christopher Barner-Kowollik (KIT/QUT) for many interesting discussions about photochemistry. M.T.L. acknowledges a PhD scholarship in context of an Alexander von Humboldt professorship for Prof. Christopher Barner-Kowollik.

Author Contributions Author Contributions Statement Conceptualization and Project Design: The corresponding author (ANU) originated the idea for the review and selected the case studies to be included. Writing—Original Draft: Both authors contributed equally to writing the manuscript. Figure Preparation & Supporting Material: All figures were selected jointly by both authors. Review & Editing: The manuscript was revised and edited by both authors to ensure scientific accuracy and clarity. Approval of Final Version: Both authors have read, approved, and accept responsibility for the final version of the manuscript and agree to be accountable for all aspects of the work.

Funding Open Access funding enabled and organized by Projekt DEAL. This study was supported by a PhD scholarship from the Alexander von Humboldt-Stiftung and the Karlsruhe Institute of Technology (KIT).

Data Availability No datasets were generated or analysed during the current study.

Declarations

Conflict of interest The authors declare no competing interests.

References

1. Polli D, Altoè P, Weingart O et al (2010) Conical intersection dynamics of the primary photoisomerization event in vision. Nature 467:440–443. https://doi.org/10.1038/nature09346
2. Li N, Ma Y, Sun W (2024) Exploring the dynamics of charge transfer in photocatalysis: applications of femtosecond transient absorption spectroscopy. Molecules 29:3995. https://doi.org/10.3390/molecules29173995
3. Wolf TJA, Fischer J, Wegener M et al (2011) Pump-probe spectroscopy on photoinitiators for stimulated-emission-depletion optical lithography. Opt Lett 36:3188–3190. https://doi.org/10.1364/OL.36.003188
4. Eigen M (1954) Methods for investigation of ionic reactions in aqueous solutions with half-times as short as 10–9 sec. Application to neutralization and hydrolysis reactions. Discuss Faraday Soc 17:194–205. https://doi.org/10.1039/DF9541700194
5. Eigen M (1967) Immeasurably fast reactions. Nobel Lect 11:1963–1979
6. Norrish RGW, Porter G (1949) Chemical reactions produced by very high light intensities. Nature 164:658–658. https://doi.org/10.1038/164658a0
7. Zewail AH (2000) Femtochemistry: atomic-scale dynamics of the chemical bond using ultrafast lasers (Nobel Lecture). Angew Chem Int Ed Engl 39:2586–2631
8. Eigen M (1996) Die" unmeßbar" schnellen Reaktionen: frühe Arbeiten (1954–1967). Thun, Frankfurt am Main
9. Quack M (2003) Von den "unmessbar schnellen" chemischen Reaktionen zur Bestimmung ultrakurzer Zeiten für chemische Primärprozesse. Akademie-Journal der Union der deutschen Akademien der Wissenschaften (Themenschwerpunkt Chemie) 1:38–44
10. Khundkar LR, Zewail AH (1990) Ultrafast molecular reaction dynamics in real-time: progress over a decade. Annu Rev Phys Chem 41:15–60
11. Shank CV (1986) Investigation of ultrafast phenomena in the femtosecond time domain. Science 233:1276–1280. https://doi.org/10.1126/science.233.4770.1276
12. Knox WH, Fork RL, Downer MC et al (1985) Optical pulse compression to 8 fs at a 5-kHz repetition rate. Appl Phys Lett 46:1120–1121. https://doi.org/10.1063/1.95728
13. Shank CV, Fork RL, Yen R et al (1982) Compression of femtosecond optical pulses. Appl Phys Lett 40:761–763. https://doi.org/10.1063/1.93276
14. Fujimoto JG, Weiner AM, Ippen EP (1984) Generation and measurement of optical pulses as short as 16 fs. Appl Phys Lett 44:832–834
15. Rosker MJ, Rose TS, Zewail AH (1988) Femtosecond real-time dynamics of photofragment-trapping resonances on dissociative potential energy surfaces. Chem Phys Lett 146:175–179. https://doi.org/10.1016/0009-2614(88)87426-8
16. Zewail AH (1988) Laser femtochemistry. Science 242:1645–1653. https://doi.org/10.1126/science.242.4886.1645
17. Sibbett W, Lagatsky AA, Brown CTA (2012) The development and application of femtosecond laser systems. Opt Express 20:6989–7001. https://doi.org/10.1364/OE.20.006989
18. Lorenc M, Ziolek M, Naskrecki R et al (2002) Artifacts in femtosecond transient absorption spectroscopy. Appl Phys B Lasers Opt 74:19–27. https://doi.org/10.1007/s003400100750
19. Bhattacharya A (2018) Ultrafast optics and spectroscopy in physical chemistry. WORLD SCIENTIFIC, New Jersey [u.a.]
20. Berera R, van Grondelle R, Kennis JTM (2009) Ultrafast transient absorption spectroscopy: principles and application to photosynthetic systems. Photosynth Res 101:105–118. https://doi.org/10.1007/s11120-009-9454-y
21. Ernsting NP, Kovalenko SA, Senyushkina T et al (2001) Wave-packet-assisted decomposition of femtosecond transient Ultraviolet−Visible absorption spectra: application to excited-state intramolecular proton transfer in solution. J Phys Chem A 105:3443–3453. https://doi.org/10.1021/jp003298o
22. Kumpulainen T, Lang B, Rosspeintner A et al (2017) Ultrafast elementary photochemical processes of organic molecules in liquid solution. Chem Rev 117:10826–10939. https://doi.org/10.1021/acs.chemrev.6b00491
23. Gerber G (1999) Die Momentaufnahme der Molekülspaltung: Chemie-Nobelpreis 1999. Phys Bl 55:23–25. https://doi.org/10.1002/phbl.19990551207
24. Rose TS, Rosker MJ, Zewail AH (1988) Femtosecond real-time observation of wave packet oscillations (resonance) in dissociation reactions. J Chem Phys 88:6672–6673. https://doi.org/10.1063/1.454408
25. Rose TS, Rosker MJ, Zewail AH (1989) Femtosecond real-time probing of reactions. IV. The reactions of alkali halides. J Chem Phys 91:7415–7436. https://doi.org/10.1063/1.457266
26. Carroll JA, Pashley-Johnson F, Klein M et al (2025) Microenvironments as an explanation for the mismatch between photochemical absorptivity and reactivity. J Am Chem Soc 147:26643–26651. https://doi.org/10.1021/jacs.5c06961
27. Strolka O, Rauthe P, Muschik T et al (2024) Continuous tuning of intersystem crossing times in Rose Bengal water/methanol solutions. J Phys Chem B 128:12189–12196. https://doi.org/10.1021/acs.jpcb.4c07449
28. Venkatraman RK, Orr-Ewing AJ (2021) Solvent effects on ultrafast photochemical pathways. Acc Chem Res 54:4383–4394. https://doi.org/10.1021/acs.accounts.1c00549
29. Zhang J, Zhu B, Zhang L et al (2023) Femtosecond transient absorption spectroscopy investigation into the electron transfer mechanism in photocatalysis. Chem Commun 59:688–699. https://doi.org/10.1039/D2CC06300J
30. Sakizadeh JD, Weiss R, Scholes GD et al (2025) Ultrafast spectroscopy and dynamics of photoredox catalysis. Annu Rev Phys Chem 76:203–229. https://doi.org/10.1146/annurev-physchem-082423-013952
31. Damrauer NH, Cerullo G, Yeh A et al (1997) Femtosecond dynamics of excited-state evolution in $[Ru(bpy)_3]^{2+}$. Science 275:54–57. https://doi.org/10.1126/science.275.5296.54
32. Valeur B, Weber G (1978) A new red-edge effect in aromatic molecules: anomaly of apparent rotation revealed by fluorescence polarization. J Chem Phys 69:2393–2400. https://doi.org/10.1063/1.436923
33. Vincent M, Gallay J, Demchenko AP (1995) Solvent relaxation around the excited state of indole: analysis of fluorescence lifetime distributions and time-dependence spectral shifts. J Phys Chem 99:14931–14941. https://doi.org/10.1021/j100041a006
34. Demchenko A P (2008) (ed) Methods in Enzymology, Academic Press
35. Demchenko AP, Sytnik AI (1991) Solvent reorganizational red-edge effect in intramolecular electron transfer. Proc Natl Acad Sci USA 88:9311–9314. https://doi.org/10.1073/pnas.88.20.9311
36. Lakowicz JR (2006) Principles of fluorescence spectroscopy. Springer, New York

37. Lakowicz JR, Keating-Nakamoto S (1984) Red-edge excitation of fluorescence and dynamic properties of proteins and membranes. Biochemistry 23:3013–3021. https://doi.org/10.1021/bi00308a026
38. Marschner DE, Frisch H, Offenloch JT et al (2018) Visible light [2 + 2] cycloadditions for reversible polymer ligation. Macromolecules 51:3802–3807. https://doi.org/10.1021/acs.macromol.8b00613
39. Menzel JP, Feist F, Tuten B et al (2019) Light-controlled orthogonal covalent bond formation at two different wavelengths. Angew Chem Int Ed Engl 58:7470–7474. https://doi.org/10.1002/anie.201901275
40. Kalayci K, Frisch H, Barner-Kowollik C et al (2020) Wavelength-dependent stiffening of hydrogel matrices via redshifted [2+2] photocycloadditions. Adv Funct Mater 30:1908171. https://doi.org/10.1002/adfm.201908171
41. Bartholomew GL, Kim SF, Oyamada Y et al (2025) Phototransposition of indazoles to benzimidazoles: tautomer-dependent reactivity, wavelength dependence, and continuous flow studies. Angew Chem Int Ed Engl 64:e202423803. https://doi.org/10.1002/anie.202423803
42. Bokosi FRB, Shiels OJ, Trevitt AJ et al (2024) Photoactivated reactions without traditional photocatalysts: electron-donor complexation of 1,2,3-Triazoles initiates denitrogenative transformations. J Org Chem 89:13243–13252. https://doi.org/10.1021/acs.joc.4c01371
43. Walden SL, Carroll JA, Unterreiner A-N et al (2024) Photochemical action plots reveal the fundamental mismatch between absorptivity and photochemical reactivity. Adv Sci 11:2306014. https://doi.org/10.1002/advs.202306014
44. Hughes RW, Lott ME, Bowman JI et al (2023) Excitation dependence in photoiniferter polymerization. ACS Macro Lett 12:14–19. https://doi.org/10.1021/acsmacrolett.2c00683
45. Ma C, Han T, Efstathiou S et al (2022) Aggregation-induced emission poly(meth)acrylates for photopatterning via wavelength-dependent visible-light-regulated controlled radical polymerization in batch and flow conditions. Macromolecules 55:9908–9917. https://doi.org/10.1021/acs.macromol.2c01413
46. Kislyak A, Frisch H, Gernhardt M et al (2020) Time-dependent differential and integral quantum yields for wavelength-dependent [4+4] photocycloadditions. Chem Eur J 26:478–484. https://doi.org/10.1002/chem.201903641
47. Gernhardt M, Blasco E, Hippler M et al (2019) Tailoring the mechanical properties of 3D microstructures using visible light post-manufacturing. Adv Mater 31:1901269. https://doi.org/10.1002/adma.201901269
48. Kanchana D, Carroll JA, Giacoletto N et al (2024) Wavelength-resolved oxime ester photoinitiator decay in radical polymerization. Macromolecules 57:9779–9787. https://doi.org/10.1021/acs.macromol.4c01980
49. Nardi M, Blasco E, Barner-Kowollik C (2022) Wavelength-resolved PhotoATRP. J Am Chem Soc 144:1094–1098. https://doi.org/10.1021/jacs.1c11259
50. Michenfelder RT, Pashley-Johnson F, Guschin V et al (2024) Photochemical action plots map orthogonal reactivity in photochemical release systems. Adv Sci 11:e2402011. https://doi.org/10.1002/advs.202402011
51. Feist F, Menzel JP, Weil T et al (2018) Visible light-induced ligation via o-quinodimethane thioethers. J Am Chem Soc 140:11848–11854. https://doi.org/10.1021/jacs.8b08343
52. Utroša P, Carroll JA, Žagar E et al (2024) Wavelength-dependent activation of photoacids and bases. Chem Eur J 30:e202400820. https://doi.org/10.1002/chem.202400820
53. Irshadeen IM, Walden SL, Wegener M et al (2021) Action plots in action: in-depth insights into photochemical reactivity. J Am Chem Soc 143:21113–21126. https://doi.org/10.1021/jacs.1c09419
54. Pashley-Johnson F, Wu X, Carroll JA et al (2025) Precision photochemistry: every photon counts. Angew Chem Int Ed 64:e202502651. https://doi.org/10.1002/anie.202502651
55. Frisch H, Marschner DE, Goldmann AS et al (2018) Wavelength-gated dynamic covalent chemistry. Angew Chem Int Ed 57:2036–2045. https://doi.org/10.1002/anie.201709991
56. Menzel JP, Noble BB, Blinco JP et al (2021) Predicting wavelength-dependent photochemical reactivity and selectivity. Nat Commun 12:1691. https://doi.org/10.1038/s41467-021-21797-x
57. Fast DE, Lauer A, Menzel JP et al (2017) Wavelength-dependent photochemistry of oxime ester photoinitiators. Macromolecules 50:1815–1823. https://doi.org/10.1021/acs.macromol.7b00089
58. Pfund B, Wenger OS (2025) Excited organic radicals in photoredox catalysis. JACS Au 5:426–447. https://doi.org/10.1021/jacsau.4c00974
59. Pfund B, Wenger OS (2025) Breaking Kasha's rule to enable higher reactivity in photoredox catalysis. J Am Chem Soc 147:26477–26485. https://doi.org/10.1021/jacs.5c06115
60. Balapure A, Ray Dutta J, Ganesan R (2024) Recent advances in semiconductor heterojunctions: A detailed review of the fundamentals of photocatalysis, charge transfer mechanism and materials. RSC Appl Interfaces 1:43–69. https://doi.org/10.1039/D3LF00126A
61. Lee Y-M, Nam W, Fukuzumi S (2023) Redox catalysis via photoinduced electron transfer. Chem Sci 14:4205–4218. https://doi.org/10.1039/D2SC07101K
62. Haken H, Wolf HC (2006) Molekülphysik und Quantenchemie, 5th edn. Springer, Berlin/Heidelberg
63. Atkins PW, Paula J (2006) Physikalische Chemie, 4 ed. WILEY-VCH, Weinheim
64. Bernath PF (2015) Spectra of Atoms and Molecules. Oxford Univ. Press, Oxford
65. Einstein A (2005) Über einen die Erzeugung und Verwandlung des Lichtes betreffenden heuristischen Gesichtspunkt [AdP 17, 132 (1905)]. Ann Phys 517:164–181. https://doi.org/10.1002/andp.2005517S111
66. Plank M (1900) Zur theorie des gesetzes der energieverteilung im normalspektrum. Verh Dtsch Phys Ges 2:237–245
67. Beer (1852) Bestimmung der Absorption des rothen Lichts in farbigen Flüssigkeiten. Ann Phys 162:78–88. https://doi.org/10.1002/andp.18521620505
68. Lambert JH (1760) Photometria sive de mensura et gradibus luminis, colorum et umbrae. sumptibus vidvae E. Klett, typis CP Detleffsen,
69. Bouguer P (1729) Essai d'optique, sur la gradation de la lumière. Claude Jombert,
70. Parnis JM, Oldham KB (2013) Beyond the Beer-Lambert law: the dependence of absorbance on time in photochemistry. J Photochem Photobiol A Chem 267:6–10. https://doi.org/10.1016/j.jphotochem.2013.06.006
71. Atkins P, Friedman R (2011) Molecular Quantum Mechanics, 5th edn. Oxford Univ. Press, Oxford
72. Wedler G, Freund H-J (2018) Lehr- und Arbeitsbuch Physikalische Chemie, 7th edn. WILEY-VCH, Weinheim
73. Dirac PAM (1927) The quantum theory of the emission and absorption of radiation. Proc R Soc A 114:243–265. https://doi.org/10.1098/rspa.1927.0039
74. Balzani V, Ceroni P, Juris A (2014) Photochemistry and photophysics: concepts, research, applications. WILEY-VCH, Weinheim
75. McQuarrie DA, Simon JD (1997) Physical chemistry: a molecular approach. Univ. Science Books, Sausalito, Kalifornien

76. Jabłoński A (1935) Über den Mechanismus der Photolumineszenz von Farbstoffphosphoren. Z Phys 94:38–46. https://doi.org/10.1007/BF01330795
77. Turro NJ, Ramamurthy V, Scaiano JC (2009) Principles of molecular photochemistry: an introduction. Univ. Science Books, Sausalito, Kalifornien
78. Rajagopal SK, Mallia AR, Hariharan M (2017) Enhanced intersystem crossing in carbonylpyrenes. Phys Chem Chem Phys 19:28225–28231. https://doi.org/10.1039/C7CP04834C
79. Kasha M (1950) Characterization of electronic transitions in complex molecules. Discuss Faraday Soc 9:14–19. https://doi.org/10.1039/DF9500900014
80. Tseng H-W, Shen J-Y, Kuo T-Y et al (2016) Excited-state intramolecular proton-transfer reaction demonstrating anti-Kasha behavior. Chem Sci 7:655–665. https://doi.org/10.1039/C5SC01945A
81. Klán P, Wirz J (2009) Photochemistry of organic compounds: from concepts to practice. Wiley, Chichester
82. Wöhrle D, Tausch MW, Stohrer W-D (2010) Photochemie: Konzepte, Methoden, Experimente. WILEY-VCH, Weinheim
83. Schweigert C, Babii O, Afonin S et al (2019) Real-time observation of Diarylethene-based photoswitches in a cyclic peptide environment. ChemPhotoChem 3:403–410. https://doi.org/10.1002/cptc.201900005
84. Michenfelder NC, Gienger C, Dilanas M et al (2020) Photoexcitation of Ge9− clusters in THF: new insights into the ultrafast relaxation dynamics and the influence of the cation. Molecules 25:2639. https://doi.org/10.3390/molecules25112639
85. Wolf TJ, Voll D, Barner-Kowollik C et al (2012) Elucidating the early steps in photoinitiated radical polymerization via femtosecond pump–probe experiments and DFT calculations. Macromolecules 45:2257–2266. https://doi.org/10.1021/ma202673q
86. Gauci SC, Du Prez FE, Holloway JO et al (2023) The power of action plots: unveiling reaction selectivity of light-stabilized dynamic covalent chemistry. Angew Chem Int Ed 62:e202310274. https://doi.org/10.1002/anie.202310274
87. Carroll JA, Pashley-Johnson F, Frisch H et al (2024) Photochemical action plots reveal red-shifted wavelength-dependent photoproduct distributions. Chem Eur J 30:e202304174. https://doi.org/10.1002/chem.202304174
88. Wald G (1968) Molecular basis of visual excitation. Science 162:230–239. https://doi.org/10.1126/science.162.3850.230
89. Yoshizawa T, Wald G (1963) Pre-lumirhodopsin and the bleaching of visual pigments. Nature 197:1279–1286. https://doi.org/10.1038/1971279a0
90. Birge RR (1981) Photophysics of light transduction in rhodopsin and bacteriorhodopsin. Annu Rev Biophys 10:315–354. https://doi.org/10.1146/annurev.bb.10.060181.001531
91. Kandori H, Shichida Y, Yoshizawa T (2001) Photoisomerization in rhodopsin. Biochem Mosc 66:1197–1209. https://doi.org/10.1023/A:1013123016803
92. Schoenlein RW, Peteanu LA, Mathies RA et al (1991) The first step in vision: femtosecond isomerization of rhodopsin. Science 254:412–415. https://doi.org/10.1126/science.1925597
93. Haran G, Morlino EA, Matthes J et al (1999) Femtosecond polarized pump−probe and stimulated emission spectroscopy of the isomerization reaction of rhodopsin. J Phys Chem A 103:2202–2207. https://doi.org/10.1021/jp9832847
94. Kochendoerfer GG, Mathies RA (1996) Spontaneous emission study of the femtosecond isomerization dynamics of rhodopsin. J Phys Chem 100:14526–14532. https://doi.org/10.1021/jp960509+
95. Busch GE, Applebury ML, Lamola AA et al (1972) Formation and decay of prelumirhodopsin at room temperatures. Proc Natl Acad Sci USA 69:2802–2806. https://doi.org/10.1073/pnas.69.10.2802
96. Shichida Y, Matuoka S, Yoshizawa T (1984) Formation of photorhodopsin, a precursor of bathorhodopsin, detected by picosecond laser photolysis at room temperature. Photobiochem Photobiophys 7:221–228. https://doi.org/10.1016/S0165-8646(24)00644-5
97. Peteanu LA, Schoenlein RW, Wang Q et al (1993) The first step in vision occurs in femtoseconds: complete blue and red spectral studies. Proc Natl Acad Sci U S A 90:11762–11766. https://doi.org/10.1073/pnas.90.24.11762
98. Hecht E, Lippert K (2018) Optik, 7 ed. De Gruyter, Berlin, Boston
99. Mathies RA, Brito Cruz CH, Pollard WT et al (1988) Direct observation of the femtosecond excited-state cis-trans isomerization in bacteriorhodopsin. Science 240:777–779
100. Song L, El-Sayed MA, Lanyi JK (1993) Protein catalysis of the retinal subpicosecond photoisomerization in the primary process of bacteriorhodopsin photosynthesis. Science 261:891–894. https://doi.org/10.1126/science.261.5123.891
101. Wang Q, Schoenlein RW, Peteanu LA et al (1994) Vibrationally coherent photochemistry in the femtosecond primary event of vision. Science 266:422–424. https://doi.org/10.1126/science.7939680
102. González-Luque R, Garavelli M, Bernardi F et al (2000) Computational evidence in favor of a two-state, two-mode model of the retinal chromophore photoisomerization. Proc Natl Acad Sci 97:9379–9384. https://doi.org/10.1073/pnas.97.17.9379
103. Garavelli M, Celani P, Bernardi F et al (1997) The C5H6NH2+ protonated Shiff base: an ab initio minimal model for retinal photoisomerization. J Am Chem Soc 119:6891–6901. https://doi.org/10.1021/ja9610895
104. Voll D, Junkers T, Barner-Kowollik C (2011) Quantitative comparison of the Mesitoyl vs the Benzoyl fragment in photoinitiation: a question of origin. Macromolecules 44:2542–2551. https://doi.org/10.1021/ma2001977
105. Günzler F, Wong EHH, Koo SPS et al (2009) Quantifying the efficiency of photoinitiation processes in Methyl Methacrylate free radical polymerization via electrospray ionization mass spectrometry. Macromolecules 42:1488–1493. https://doi.org/10.1021/ma802308z
106. Arsu N, Reetz I, Yagci Y et al (2009) Photoinitiated radical vinyl polymerization. CRC Press Taylor & Francis Group, New York
107. Yağci Y, Reetz I (1998) Externally stimulated initiator systems for cationic polymerization. Prog Polym Sci 23:1485–1538. https://doi.org/10.1016/S0079-6700(98)00010-0
108. Kutal C, Grutsch PA, Yang DB (1991) A novel strategy for photoinitiated anionic polymerization. Macromolecules 24:6872–6873
109. Gruber HF (1992) Photoinitiators for free radical polymerization. Prog Polym Sci 17:953–1044. https://doi.org/10.1016/0079-6700(92)90006-K
110. Hageman HJ (1985) Photoinitiators for free radical polymerization. Prog Org Coat 13:123–150. https://doi.org/10.1016/0033-0655(85)80021-2
111. Arsu N, Aydin M, Yagci Y et al (2006) One component thioxanthone based Type II photoinitiators. Photochemistry and UV curing: new trends1–13.
112. Wang W, Jin M, Pan H et al (2021) Remote effect of substituents on the properties of phenyl thienyl thioether-based oxime esters as LED-sensitive photoinitiators. Dyes Pigm 192:109435. https://doi.org/10.1016/j.dyepig.2021.109435
113. Yilmaz G, Tuzun A, Yagci Y (2010) Thioxanthone–carbazole as a visible light photoinitiator for free radical polymerization. J Polym Sci A Polym Chem 48:5120–5125. https://doi.org/10.1002/pola.24310
114. Jankowiak A, Kaszynski P (2009) 4-Substituted 1-Acyloxypyridine-2(1H)-thiones: experimental and computational studies of the substituent effect on electronic absorption spectra. J Org Chem 74:7441–7448. https://doi.org/10.1021/jo901522r

115. Pawelka Z, Kryachko ES, Zeegers-Huyskens T (2003) Theoretical and experimental study of the conformational and vibrational properties of benzoin. Chem Phys 287:143–153. https://doi.org/10.1016/S0301-0104(02)00986-2
116. Lipson M, Turro NJ (1996) Picosecond investigation of the effect of solvent on the photochemistry of benzoin. J Photochem Photobiol A Chem 99:93–96. https://doi.org/10.1016/S1010-6030(96)04399-7
117. Shrestha NK, Yagi EJ, Takatori Y et al (1998) Photochemical α-cleavage reaction of benzoin and its derivatives. J Photochem Photobiol A Chem 116:179–185. https://doi.org/10.1016/S1010-6030(98)00308-6
118. Lewis F, Lauterbach R, Heine H et al (1975) Photochemical. alpha. cleavage of benzoin derivatives. Polar transition states for free-radical formation. J Am Chem Soc 97:1519–1525
119. Ma C, Du Y, Kwok WM et al (2007) Femtosecond transient absorption and nanosecond time-resolved resonance Raman study of the solvent-dependent photo-deprotection reaction of Benzoin Diethyl Phosphate. Chem Eur J 13:2290–2305. https://doi.org/10.1002/chem.200600893
120. Fisher JP, Dean D, Engel PS et al (2001) Photoinitiated polymerization of biomaterials. Annu Rev Mater Res 31:171–181. https://doi.org/10.1146/annurev.matsci.31.1.171
121. Anseth KS, Metters AT, Bryant SJ et al (2002) In situ forming degradable networks and their application in tissue engineering and drug delivery. J Control Release 78:199–209. https://doi.org/10.1016/S0168-3659(01)00500-4
122. Sun H-B, Kawata S (2004). In: Fatkullin N, Ikehara T, Jinnai H, Kawata S, Kimmich R, Nishi T, Nishikawa Y, Sun HB (eds) NMR • 3D Analysis • Photopolymerization. Springer, Berlin, Heidelberg
123. Jöckle P, Lamparth I, Moszner N et al (2020) Evidence for ultrafast formation of tribenzoylgermyl radicals originating from tetraacylgermane photoinitiators. Polym Chem 11:3972–3979. https://doi.org/10.1039/D0PY00344A
124. Billiet T, Vandenhaute M, Schelfhout J et al (2012) A review of trends and limitations in hydrogel-rapid prototyping for tissue engineering. Biomater 33:6020–6041. https://doi.org/10.1016/j.biomaterials.2012.04.050
125. Nguyen KT, West JL (2002) Photopolymerizable hydrogels for tissue engineering applications. Biomater 23:4307–4314. https://doi.org/10.1016/S0142-9612(02)00175-8
126. Fischer J, von Freymann G, Wegener M (2010) The materials challenge in diffraction-unlimited direct-laser-writing optical lithography. Adv Mater 22:3578–3582. https://doi.org/10.1002/adma.201000892
127. Dietliker K, Hüsler R, Birbaum JL et al (2007) Advancements in photoinitiators—opening up new applications for radiation curing. Prog Org Coat 58:146–157. https://doi.org/10.1016/j.porgcoat.2006.08.021
128. Karasu F, Croutxé-Barghorn C, Allonas X et al (2014) Free radical photopolymerization initiated by UV and LED: towards UV stabilized, tack free coatings. J Polym Sci A Polym Chem 52:3597–3607. https://doi.org/10.1002/pola.27427
129. Moszner N, Fischer UK, Ganster B et al (2008) Benzoyl Germanium derivatives as novel visible light photoinitiators for dental materials. Dent Mater 24:901–907. https://doi.org/10.1016/j.dental.2007.11.004
130. Bruschi C, Gui X, Rauthe P et al (2024) Dual role of a novel heteroleptic Cu(I) complex in visible-light-driven CO2 reduction. Chem Eur J 30:e202400765. https://doi.org/10.1002/chem.202400765
131. Leier J, Rauthe P, Tabone R et al (2024) Excited state dynamics of homoleptic Zn(ii)dipyrrin complexes and their application in photocatalysis. New J Chem 48:13261–13269. https://doi.org/10.1039/d4nj02527j
132. Wenzel JO, Werner J, Allgaier A et al (2024) Visible-Light activation of Diorganyl Bis(pyridylimino) Isoindolide Aluminum(III) complexes and their organometallic radical reactivity. Angew Chem Int Ed 63:e202402885. https://doi.org/10.1002/anie.202402885
133. Zhang L, Mohamed HH, Dillert R et al (2012) Kinetics and mechanisms of charge transfer processes in photocatalytic systems: a review. J Photochem Photobiol C Photochem Rev 13:263–276. https://doi.org/10.1016/j.jphotochemrev.2012.07.002
134. Zhang Y, Lee TS, Favale JM et al (2020) Delayed fluorescence from a Zirconium(iv) photosensitizer with ligand-to-metal charge-transfer excited states. Nat Chem 12:345–352. https://doi.org/10.1038/s41557-020-0430-7
135. Takeda H, Ohashi K, Sekine A et al (2016) Photocatalytic CO2 reduction using Cu(I) photosensitizers with a Fe(II) catalyst. J Am Chem Soc 138:4354–4357. https://doi.org/10.1021/jacs.6b01970
136. Yuan H, Du J, Ming M et al (2022) Combination of organic dye and iron for CO2 reduction with pentanuclear Fe2Na3 Purpurin photocatalysts. J Am Chem Soc 144:4305–4309. https://doi.org/10.1021/jacs.1c13081
137. Wang J-W, Li Z, Luo Z-M et al (2023) Boosting CO2 photoreduction by π–π-induced preassembly between a Cu(I) sensitizer and a pyrene-appended Co(II) catalyst. Proc Natl Acad Sci U S A 120:e2221219120. https://doi.org/10.1073/pnas.2221219120
138. Luo S-P, Mejía E, Friedrich A et al (2013) Photocatalytic water reduction with Copper-Based photosensitizers: a noble-metal-free system. Angew Chem Int Ed 52:419–423. https://doi.org/10.1002/anie.201205915
139. Junge H, Rockstroh N, Fischer S et al (2017) Light to hydrogen: photocatalytic hydrogen generation from water with molecularly-defined iron complexes. Inorganics 5:14. https://doi.org/10.3390/inorganics5010014
140. Giereth R, Reim I, Frey W et al (2019) Remarkably long-lived excited states of copper photosensitizers containing an extended π-system based on an anthracene moiety. Sustain Energy Fuels 3:692–700. https://doi.org/10.1039/C8SE00521D
141. Housecroft CE, Constable EC (2022) Solar energy conversion using first row d-block metal coordination compound sensitizers and redox mediators. Chem Sci 13:1225–1262. https://doi.org/10.1039/D1SC06828H
142. Housecroft CE, Constable EC (2015) The emergence of copper(i)-based dye sensitized solar cells. Chem Soc Rev 44:8386–8398. https://doi.org/10.1039/C5CS00215J
143. Chen N-Y, Xia L-M, Lennox AJJ et al (2017) Structure-activated copper photosensitisers for photocatalytic water reduction. Chem Eur J 23:3631–3636. https://doi.org/10.1002/chem.201602598
144. Mejía E, Luo S-P, Karnahl M et al (2013) A noble-metal-free system for photocatalytic hydrogen production from water. Chem Eur J 19:15972–15978. https://doi.org/10.1002/chem.201302091
145. Lennox AJJ, Fischer S, Jurrat M et al (2016) Copper-based photosensitisers in water reduction: a more efficient in situ formed system and improved mechanistic understanding. Chem Eur J 22:1233–1238. https://doi.org/10.1002/chem.201503812
146. Windisch J, Orazietti M, Hamm P et al (2016) General scheme for oxidative quenching of a copper bis-phenanthroline photosensitizer for light-driven hydrogen production. Chemsuschem 9:1719–1726. https://doi.org/10.1002/cssc.201600422
147. Kim J, Whang DR, Park SY (2017) Designing highly efficient CuI photosensitizers for photocatalytic H2 evolution from water. Chemsuschem 10:1883–1886. https://doi.org/10.1002/cssc.201700389
148. Karnahl M, Mejía E, Rockstroh N et al (2014) Photocatalytic hydrogen production with copper photosensitizer-titanium dioxide composites. ChemCatChem 6:82–86. https://doi.org/10.1002/cctc.201300459

149. Zhang Y, Zedler L, Karnahl M et al (2019) Excited-state dynamics of heteroleptic copper(i) photosensitizers and their electrochemically reduced forms containing a dipyridophenazine moiety – a spectroelectrochemical transient absorption study. Phys Chem Chem Phys 21:10716–10725. https://doi.org/10.1039/C9CP00412B
150. Symes MD, Cronin L (2013) Decoupling hydrogen and oxygen evolution during electrolytic water splitting using an electron-coupled-proton buffer. Nat Chem 5:403–409. https://doi.org/10.1038/nchem.1621
151. Karlsson S, Boixel J, Pellegrin Y et al (2012) Accumulative electron transfer: multiple charge separation in artificial photosynthesis. Faraday Discuss 155:233–252. https://doi.org/10.1039/C1FD00089F
152. Sueyoshi F, Zhang X, Yamauchi K et al (2023) Controlling the photofunctionality of a polyanionic heteroleptic Copper(I) photosensitizer for CO2 reduction using its ion-pair formation with polycationic ammonium in aqueous media. Angew Chem Int Ed 62:e202217807. https://doi.org/10.1002/anie.202217807
153. Kuramochi Y, Sato R, Sakuma H et al (2022) Photocatalytic CO2 reduction sensitized by a special-pair mimic porphyrin connected with a rhenium(i) tricarbonyl complex. Chem Sci 13:9861–9879. https://doi.org/10.1039/D2SC03251A
154. Wang J-W, Ma F, Jin T et al (2023) Homoleptic Al(III) photosensitizers for durable CO2 photoreduction. J Am Chem Soc 145:676–688
155. Wegeberg C, Häussinger D, Kupfer S et al (2024) Controlling the Photophysical Properties of a Series of Isostructural d6 Complexes Based on Cr0, MnI, and FeII. J Am Chem Soc 146:4605–4619
156. Aydogan A, Bangle RE, Cadranel A et al (2021) Accessing photoredox transformations with an Iron(III) photosensitizer and green light. J Am Chem Soc 143:15661–15673. https://doi.org/10.1021/jacs.1c06081
157. Zhang Y, Schulz M, Wächtler M et al (2018) Heteroleptic diimine–diphosphine Cu(I) complexes as an alternative towards noble-metal based photosensitizers: design strategies, photophysical properties and perspective applications. Coord Chem Rev 356:127–146. https://doi.org/10.1016/j.ccr.2017.10.016
158. Forero Cortés PA, Marx M, Trose M et al (2021) Heteroleptic copper complexes with nitrogen and phosphorus ligands in photocatalysis: overview and perspectives. Chem Catal 1:298–338. https://doi.org/10.1016/j.checat.2021.05.005
159. Hossain A, Bhattacharyya A, Reiser O (2019) Copper's rapid ascent in visible-light photoredox catalysis. Science 364:eaav9713. https://doi.org/10.1126/science.aav9713
160. Dietrich-Buchecker CO, Marnot PA, Sauvage J-P et al (1983) Bis(2,9-diphenyl-1,10-phenanthroline)copper(I): a copper complex with a long-lived charge-transfer excited state. J Chem Soc, Chem Commun. https://doi.org/10.1039/C39830000513
161. Cuttell DG, Kuang S-M, Fanwick PE et al (2002) Simple Cu(I) Complexes with Unprecedented Excited-State Lifetimes. J Am Chem Soc 124:6–7
162. Reiser O (2016) Shining light on copper: unique opportunities for visible-light-catalyzed atom transfer radical addition reactions and related processes. Acc Chem Res 49:1990–1996. https://doi.org/10.1021/acs.accounts.6b00296
163. Eberhart MS, Phelan BT, Niklas J et al (2020) Surface immobilized copper(i) diimine photosensitizers as molecular probes for elucidating the effects of confinement at interfaces for solar energy conversion. Chem Commun 56:12130–12133. https://doi.org/10.1039/D0CC05972B
164. Zhang Y, Traber P, Zedler L et al (2018) Cu(i) vs. Ru(ii) photosensitizers: elucidation of electron transfer processes within a series of structurally related complexes containing an extended π-system. Phys Chem Chem Phys 20:24843–24857. https://doi.org/10.1039/C8CP04595J
165. Armaroli N (2001) Photoactive mono- and polynuclear Cu(i)–phenanthrolines. A viable alternative to Ru(ii)–polypyridines? Chem Soc Rev 30:113–124. https://doi.org/10.1039/B000703J
166. Förster C, Heinze K (2020) Photophysics and photochemistry with Earth-abundant metals – fundamentals and concepts. Chem Soc Rev 49:1057–1070. https://doi.org/10.1039/C9CS00573K
167. Schulz M, Reichardt C, Müller C et al (2017) Excited state properties of heteroleptic Cu(I) 4H-Imidazolate complexes. Inorg Chem 56:12978–12986. https://doi.org/10.1021/acs.inorgchem.7b01680
168. Iwamura M, Takeuchi S, Tahara T (2015) Ultrafast excited-state dynamics of copper(I) complexes. Acc Chem Res 48:782–791. https://doi.org/10.1021/ar500353h
169. Lazorski MS, Castellano FN (2014) Advances in the light conversion properties of Cu(I)-based photosensitizers. Polyhedron 82:57–70. https://doi.org/10.1016/j.poly.2014.04.060
170. Rosas-Hernández A, Steinlechner C, Junge H et al (2017) Earth-abundant photocatalytic systems for the visible-light-driven reduction of CO2 to CO. Green Chem 19:2356–2360. https://doi.org/10.1039/C6GC03527B
171. Rader RA, Matthews G (1981) Photostudies of [Cu (bpy)(PPh3) 2]+,[C~(phen)(PPh~)~]+, and [C~(dmp)(PPh~)~]+ in solution and in rigid, low-temperature glasses. Simultaneous multiple emissions from intraligand and charge-transfer states'. J Am Chem Soc 103:5906–5912
172. Kirchhoff JR, McMillin DR, Robinson WR et al (1985) Steric effects and the behavior of Cu (NN)(PPh3) 2+ systems in fluid solution. Crystal and molecular structures of [Cu (dmp)(PPh3) 2] NO3 and [Cu (phen)(PPh3) 2] NO3. 1.5 EtOH. Inorg Chem 24:3928–3933. https://doi.org/10.1021/ic00217a047
173. Del Paggio AA, McMillin DR (1983) Substituent effects and the photoluminescence of Cu (PPh3) 2 (NN)+ systems. Inorg Chem 22:691–692. https://doi.org/10.1021/ic00146a024
174. Eggleston MK, McMillin DR, Koenig KS et al (1997) Steric effects in the ground and excited states of Cu(NN)2+ systems. Inorg Chem 36:172–176. https://doi.org/10.1021/ic960698a
175. Ichinaga AK, Kirchhoff JR, McMillin DR et al (1987) Charge-transfer absorption and emission of Cu (NN) 2+ systems. Inorg Chem 26:4290–4292. https://doi.org/10.1021/ic00272a030
176. Everly RM, McMillin DR (1989) Concentration-dependent lifetimes of Cu(NN)+2 systems: exciplex quenching from the ion pair state. Photochem Photobiol 50:711–716. https://doi.org/10.1111/j.1751-1097.1989.tb02900.x
177. Buckner MT, McMillin DR (1978) Photoluminescence from copper (I) complexes with low-lying metal-to-ligand charge transfer excited states. J Chem Soc, Chem Commun759–761.
178. Hayes D, Kohler L, Chen LX et al (2018) Ligand mediation of vectorial charge transfer in Cu(I)diimine chromophore–acceptor dyads. J Phys Chem Lett 9:2070–2076. https://doi.org/10.1021/acs.jpclett.8b00468
179. Argüello Cordero MA, Boden PJ, Rentschler M et al (2022) Comprehensive picture of the excited state dynamics of Cu(I)- and Ru(II)-based photosensitizers with long-lived triplet states. Inorg Chem 61:214–226. https://doi.org/10.1021/acs.inorgchem.1c02771
180. Yamazaki Y, Takeda H, Ishitani O (2015) Photocatalytic reduction of CO2 using metal complexes. J Photochem Photobiol C Photochem Rev 25:106–137. https://doi.org/10.1016/j.jphotochemrev.2015.09.001
181. Berardi S, Drouet S, Francàs L et al (2014) Molecular artificial photosynthesis. Chem Soc Rev 43:7501–7519. https://doi.org/10.1039/C3CS60405E
182. Wang J-W, Jiang L, Huang H-H et al (2021) Rapid electron transfer via dynamic coordinative interaction boosts quantum efficiency

for photocatalytic CO2 reduction. Nat Commun 12:4276. https://doi.org/10.1038/s41467-021-24647-y
183. Takeda H, Monma Y, Sugiyama H et al (2019) Development of visible-light driven Cu(I) complex photosensitizers for photocatalytic CO2 reduction. Front Chem 7:2019. https://doi.org/10.3389/fchem.2019.00418
184. Ruthkosky M, Kelly CA, Castellano FN et al (1998) Electron and energy transfer from CuI MLCT excited states. Coord Chem Rev 171:309–322. https://doi.org/10.1016/S0010-8545(98)90045-5
185. Xie Z-L, Gupta N, Niklas J et al (2023) Photochemical charge accumulation in a heteroleptic copper(i)-anthraquinone molecular dyad via proton-coupled electron transfer. Chem Sci 14:10219–10235. https://doi.org/10.1039/D3SC03428C
186. Singh S, de Tacconi NR, Diaz NRG et al (2011) Photochemical two-electron reduction of a dinuclear ruthenium complex containing a bent tetraazatetrapyridopentacene bridging ligand: pushing up the LUMO for storing more energy. Inorg Chem 50:9318–9328. https://doi.org/10.1021/ic2006698
187. Tschierlei S, Karnahl M, Rockstroh N et al (2014) Substitution-controlled excited state processes in heteroleptic Copper(I) photosensitizers used in hydrogen evolving systems. ChemPhysChem 15:3709–3713. https://doi.org/10.1002/cphc.201402585
188. Heberle M, Tschierlei S, Rockstroh N et al (2017) Heteroleptic Copper photosensitizers: why an extended π-system does not automatically lead to enhanced hydrogen production. Chem Eur J 23:312–319. https://doi.org/10.1002/chem.201604005
189. Fransted KA, Jackson NE, Zong R et al (2014) Ultrafast structural dynamics of Cu(I)-bicinchoninic acid and their implications for solar energy applications. J Phys Chem A 118:10497–10506. https://doi.org/10.1021/jp504294j
190. Kohler L, Hadt RG, Hayes D et al (2017) Synthesis, structure, and excited state kinetics of heteroleptic Cu(i) complexes with a new sterically demanding phenanthroline ligand. Dalton Trans 46:13088–13100. https://doi.org/10.1039/C7DT02476B
191. Ruiz GT, Juliarena MP, Lezna RO et al (2006) On the parallel formation of long-lived excited states of dipyridil[3,2-a:2′3′-c] phenazine, dppz: a contrast between the electrochemically and photochemically induced reduction of dppz. J Photochem Photobiol A Chem 179:289–297. https://doi.org/10.1016/j.jphotochem.2005.07.024
192. Berger S, Fiedler J, Reinhardt R et al (2004) Metal vs ligand reduction in complexes of Dipyrido[3,2-a:2‘,3‘-c]phenazine and related ligands with [(C5Me5)ClM]+ (M = Rh or Ir): evidence for potential rather than orbital control in the reductive cleavage of the metal−chloride bond. Inorg Chem 43:1530–1538. https://doi.org/10.1021/ic0351388
193. Ponseca CS Jr., Chábera P, Uhlig J et al (2017) Ultrafast electron dynamics in solar energy conversion. Chem Rev 117:10940–11024. https://doi.org/10.1021/acs.chemrev.6b00807
194. Juliarena MP, Lezna RO, Feliz MR et al (2006) On the association and structure of radicals derived from Dipyridil[3,2-a:2‘3‘-c] phenazine. Contrast between the electrochemical, radiolytic, and photochemical reduction processes. J Org Chem 71:2870–2873. https://doi.org/10.1021/jo051985b
195. McGovern DA, Selmi A, O’Brien JE et al (2005) Reduction of dipyrido-[3,2-a:2′,3′-c]-phenazine (dppz) by photolysis in ethanol solution. Chem Commun. https://doi.org/10.1039/B415471A
196. McCusker JK (2019) Electronic structure in the transition metal block and its implications for light harvesting. Science 363:484–488. https://doi.org/10.1126/science.aav9104
197. Wegeberg C, Wenger OS (2021) Luminescent first-row transition metal complexes. JACS Au 1:1860–1876. https://doi.org/10.1021/jacsau.1c00353
198. Yarranton JT, McCusker JK (2022) Ligand-field spectroscopy of Co(III) complexes and the development of a spectrochemical series for low-spin d6 charge-transfer chromophores. J Am Chem Soc 144:12488–12500. https://doi.org/10.1021/jacs.2c04945
199. Alowakennu MM, Ghosh A, McCusker JK (2023) Direct evidence for excited ligand field state-based oxidative photoredox chemistry of a Cobalt(III) polypyridyl photosensitizer. J Am Chem Soc 145:20786–20791. https://doi.org/10.1021/jacs.3c09374
200. Chan AY, Ghosh A, Yarranton JT et al (2023) Exploiting the Marcus inverted region for first-row transition metal–based photoredox catalysis. Science 382:191–197. https://doi.org/10.1126/science.adj0612
201. Yaltseva P, Wenger OS (2023) Photocatalysis gets energized by abundant metals. Science 382:153–154. https://doi.org/10.1126/science.adk5923
202. Zhang K, Ash R, Girolami GS et al (2019) Tracking the metal-centered triplet in photoinduced spin crossover of Fe(phen)32+ with tabletop femtosecond M-Edge x-ray absorption near-edge structure spectroscopy. J Am Chem Soc 141:17180–17188. https://doi.org/10.1021/jacs.9b07332
203. Juban EA, Smeigh AL, Monat JE et al (2006) Ultrafast dynamics of ligand-field excited states. Coord Chem Rev 250:1783–1791. https://doi.org/10.1016/j.ccr.2006.02.010
204. Sousa C, de Graaf C, Rudavskyi A et al (2013) Ultrafast deactivation mechanism of the excited singlet in the light-induced spin crossover of [Fe(2,2′-bipyridine)3]2+. Chem Eur J 19:17541–17551. https://doi.org/10.1002/chem.201302992
205. Liu Y, Persson P, Sundström V et al (2016) Fe N-heterocyclic carbene complexes as promising photosensitizers. Acc Chem Res 49:1477–1485. https://doi.org/10.1021/acs.accounts.6b00186
206. Ting SI, Garakyaraghi S, Taliaferro CM et al (2020) 3d-d excited states of Ni(II) complexes relevant to photoredox catalysis: Spectroscopic identification and mechanistic implications. J Am Chem Soc 142:5800–5810. https://doi.org/10.1021/jacs.0c00781
207. Sinha N, Wenger OS (2023) Photoactive metal-to-ligand charge transfer excited states in 3d6 complexes with Cr0, MnI, FeII, and CoIII. J Am Chem Soc 145:4903–4920. https://doi.org/10.1021/jacs.2c13432
208. Liu Y, Harlang T, Canton SE et al (2013) Towards longer-lived metal-to-ligand charge transfer states of iron(ii) complexes: An N-heterocyclic carbene approach. Chem Commun 49:6412–6414. https://doi.org/10.1039/C3CC43833C
209. Duchanois T, Etienne T, Cebrián C et al (2015) An Iron-based photosensitizer with extended excited-state lifetime: photophysical and photovoltaic properties. Eur J Inorg Chem 2015:2469–2477. https://doi.org/10.1002/ejic.201500142
210. Liu L, Duchanois T, Etienne T et al (2016) A new record excited state 3MLCT lifetime for metalorganic iron(ii) complexes. Phys Chem Chem Phys 18:12550–12556. https://doi.org/10.1039/C6CP01418F
211. Sinha N, Wegeberg C, Häussinger D et al (2023) Photoredox-active Cr(0) luminophores featuring photophysical properties competitive with Ru(II) and Os(II) complexes. Nat Chem 15:1730–1736. https://doi.org/10.1038/s41557-023-01297-9
212. Narayanam JMR, Stephenson CRJ (2011) Visible light photoredox catalysis: Applications in organic synthesis. Chem Soc Rev 40:102–113. https://doi.org/10.1039/B913880N
213. Shaw MH, Twilton J, MacMillan DWC (2016) Photoredox catalysis in organic chemistry. J Org Chem 81:6898–6926. https://doi.org/10.1021/acs.joc.6b01449
214. Wenger OS (2018) Photoactive complexes with earth-abundant metals. J Am Chem Soc 140:13522–13533. https://doi.org/10.1021/jacs.8b08822
215. Campagna S, Puntoriero F, Nastasi F et al (2007). In: Balzani V, Campagna S (eds) Photochemistry and Photophysics of Coordination Compounds I. Springer, Berlin, Heidelberg

216. Pal AK, Hanan GS (2014) Design, synthesis and excited-state properties of mononuclear Ru(ii) complexes of tridentate heterocyclic ligands. Chem Soc Rev 43:6184–6197. https://doi.org/10.1039/C4CS00123K
217. Kusaka S, Sakamoto R, Kitagawa Y et al (2012) An extremely bright heteroleptic Bis(dipyrrinato)zinc(II) complex. Chem Asian J 7:907–910. https://doi.org/10.1002/asia.201200131
218. Kögel JF, Kusaka S, Sakamoto R et al (2016) Heteroleptic [Bis (oxazoline)](dipyrrinato) zinc (II) complexes: bright and circularly polarized luminescence from an originally achiral dipyrrinato ligand. Angew Chem Int Ed Engl 55:1377. https://doi.org/10.1002/ange.201509411
219. Trinh C, Kirlikovali K, Das S et al (2014) Symmetry-breaking charge transfer of visible light absorbing systems: Zinc dipyrrins. J Phys Chem C 118:21834–21845. https://doi.org/10.1021/jp506855t
220. Antina EV, Berezin MB, Dudina NA et al (2014) Synthesis, spectral-luminescent properties of B(III) and Zn(II) complexes with alkyl- and aryl-substituted dipyrrins and azadipyrrins. Russ J Inorg Chem 59:1187–1194. https://doi.org/10.1134/S0036023614100027
221. Alqahtani NZ, Blevins TG, McCusker CE (2019) Quantifying triplet state formation in Zinc dipyrrin complexes. J Phys Chem A 123:10011–10018. https://doi.org/10.1021/acs.jpca.9b08682
222. Niedzwiedzki DM, Chatterjee N, Enriquez MM et al (2009) Spectroscopic investigation of Peridinin analogues having different π-electron conjugated chain lengths: Exploring the nature of the intramolecular charge transfer state. J Phys Chem B 113:13604–13612. https://doi.org/10.1021/jp903923r
223. Kellogg M, Akil A, Muthiah Ravinson DS et al (2019) Symmetry breaking charge transfer as a means to study electron transfer with no driving force. Faraday Discuss 216:379–394. https://doi.org/10.1039/C8FD00201K
224. Sartor SM, Lattke YM, McCarthy BG et al (2019) Effects of Naphthyl connectivity on the photophysics of compact organic charge-transfer photoredox catalysts. J Phys Chem A 123:4727–4736. https://doi.org/10.1021/acs.jpca.9b03286
225. Hammarström L (2015) Accumulative charge separation for solar fuels production: Coupling light-induced single electron transfer to multielectron catalysis. Acc Chem Res 48:840–850. https://doi.org/10.1021/ar500386x
226. Bessette A, Hanan GS (2014) Design, synthesis and photophysical studies of dipyrromethene-based materials: insights into their applications in organic photovoltaic devices. Chem Soc Rev 43:3342–3405. https://doi.org/10.1039/C3CS60411J
227. Asaoka M, Kitagawa Y, Teramoto R et al (2017) Theoretical study on S1 and T1 states of homoleptic bis(dipyrrinato)zinc(II) model complex. Polyhedron 136:113–116. https://doi.org/10.1016/j.poly.2017.01.058
228. Bartynski AN, Gruber M, Das S et al (2015) Symmetry-breaking charge transfer in a Zinc chlorodipyrrin acceptor for high open circuit voltage organic photovoltaics. J Am Chem Soc 137:5397–5405. https://doi.org/10.1021/jacs.5b00146
229. Sakamoto R, Iwashima T, Kögel JF et al (2016) Dissymmetric Bis(dipyrrinato)zinc(II) complexes: Rich variety and bright red to near-infrared luminescence with a large Pseudo-Stokes shift. J Am Chem Soc 138:5666–5677. https://doi.org/10.1021/jacs.6b02128
230. Kübler JA, Pfund B, Wenger OS (2022) Zinc(II) complexes with triplet charge-transfer excited states enabling energy-transfer catalysis, photoinduced electron transfer, and upconversion. JACS Au 2:2367–2380. https://doi.org/10.1021/jacsau.2c00442
231. Giuso V, Jouaiti E, Cebrián C et al (2023) Symmetry-broken charge-transfer excited state in homoleptic Zinc(II) Imidazo[1,2-a]pyridine complexes. ChemPhotoChem 7:e202300092. https://doi.org/10.1002/cptc.202300092
232. Kuznetsova RT, Aksenova YV, Bashkirtsev DE et al (2015) Photonics of zinc(II) and boron(III) chelates with methyl- and phenyl-substituted dipyrromethenes and azadipyrromethenes. High Energy Chem 49:16–23
233. Yu L, Muthukumaran K, Sazanovich IV et al (2003) Excited-state energy-transfer dynamics in self-assembled triads composed of two porphyrins and an intervening bis(dipyrrinato)metal complex. Inorg Chem 42:6629–6647. https://doi.org/10.1021/ic034559m
234. Tsuchiya M, Sakamoto R, Kusaka S et al (2013) Triarylamine-conjugated bis(dipyrrinato)zinc(II) complexes: impact of Triarylamine on photochemical property and multi-redox reaction. Electrochemistry 81:337–339. https://doi.org/10.5796/electrochemistry.81.337
235. Sazanovich IV, Kirmaier C, Hindin E et al (2004) Structural control of the excited-state dynamics of bis(dipyrrinato)zinc complexes: self-assembling chromophores for light-harvesting architectures. J Am Chem Soc 126:2664–2665. https://doi.org/10.1021/ja038763k
236. Gahlaut PS, Yadav K, Gautam D et al (2022) Recent developments in the syntheses of Aluminum complexes based on redox-active ligands. J Organomet Chem 963:122298. https://doi.org/10.1016/j.jorganchem.2022.122298
237. Mandal D, Demirer TI, Sergeieva T et al (2023) Evidence of AlII radical addition to Benzene. Angew Chem Int Ed Engl 62:e202217184. https://doi.org/10.1002/anie.202217184
238. Nakamoto M, Yamasaki T, Sekiguchi A (2005) Stable mononuclear radical anions of heavier Group 13 elements: [(tBu2MeSi)3E•-]·[K+(2.2.2-Cryptand)] (E = Al, Ga). J Am Chem Soc 127:6954–6955. https://doi.org/10.1021/ja051814o
239. Li B, Kundu S, Stückl AC et al (2017) A Stable Neutral Radical in the Coordination Sphere of Aluminum. Angew Chem Int Ed 56:397–400. https://doi.org/10.1002/anie.201609101
240. Hobson K, Carmalt CJ, Bakewell C (2020) Recent advances in low oxidation state aluminium chemistry. Chem Sci 11:6942–6956. https://doi.org/10.1039/D0SC02686G
241. Bakewell C, Hobson K, Carmalt CJ (2022) Exploring equilibria between Aluminium(I) and Aluminium(III): the formation of dihydroalanes, masked dialumenes and Aluminium(I) species. Angew Chem Int Ed Engl 61:e202205901. https://doi.org/10.1002/anie.202205901
242. Zhang X, Mei Y, Liu LL (2022) Free Aluminylenes: an emerging class of compounds. Chem Eur J 28:e202202102. https://doi.org/10.1002/chem.202202102
243. Liu J, Lu L, Wood D et al (2020) New redox strategies in organic synthesis by means of electrochemistry and photochemistry. ACS Cent Sci 6:1317–1340. https://doi.org/10.1021/acscentsci.0c00549
244. Gavin JT, Belli RG, Roberts CC (2022) Radical-polar crossover catalysis with a d0 metal enabled by a redox-active ligand. J Am Chem Soc 144:21431–21436. https://doi.org/10.1021/jacs.2c09114
245. Vogler A, Paukner A, Kunkely H (1990) Photochemistry of coordination compounds of the main group metals. Coord Chem Rev 97:285–297. https://doi.org/10.1016/0010-8545(90)80096-C
246. Vogler A, Nikol H (1992) Photochemistry and photophysics of coordination compounds of the main group metals. Pure Appl Chem 64:1311–1317
247. Nakada A, Matsumoto T, Chang H-C (2022) Redox-active ligands for chemical, electrochemical, and photochemical molecular conversions. Coord Chem Rev 473:214804. https://doi.org/10.1016/j.ccr.2022.214804
248. Liu Z, Zhang X, Zhang Y et al (2007) Theoretical investigation of the molecular, electronic structures and vibrational spectra of a series of first transition metal phthalocyanines. Spectrochim Acta

A Mol Biomol Spectrosc 67:1232–1246. https://doi.org/10.1016/j.saa.2006.10.013
249. Siegl WO (1977) Metal ion activation of nitriles. Syntheses of 1, 3-bis (arylimino) isoindolines. J Org Chem 42:1872–1878. https://doi.org/10.1021/jo00431a011
250. Wenzel JO, Fernández I, Breher F (2023) Synthesis and characterization of Bis(pyridylimino)isoindolide alkali metal complexes in three redox states. Eur J Inorg Chem 26:e202300315. https://doi.org/10.1002/ejic.202300315
251. Knijnenburg Q, Smits JMM, Budzelaar PHM (2006) Reaction of the diimine pyridine ligand with aluminum alkyls: an unexpectedly complex reaction. Organometallics 25:1036–1046. https://doi.org/10.1021/om050936m
252. Gallardo-Villagrán M, Vidal F, Palma P et al (2019) Aluminium(iii) dialkyl 2,6-bisimino-4R-dihydropyridinates(−1): selective synthesis, structure and controlled dimerization. Dalton Trans 48:9104–9116. https://doi.org/10.1039/C9DT00847K
253. Knijnenburg Q, Gambarotta S, Budzelaar PHM (2006) Ligand-centred reactivity in diiminepyridine complexes. Dalton Trans. https://doi.org/10.1039/B612251E
254. Ke M-R, Chen Z, Shi J et al (2023) A smart and visible way to switch the aromaticity of silicon(iv) phthalocyanines. Chem Commun 59:9832–9835. https://doi.org/10.1039/D3CC02910G
255. Iwamura M, Takeuchi S, Tahara T (2007) Real-time observation of the photoinduced structural change of Bis(2,9-dimethyl-1,10-phenanthroline)copper(I) by femtosecond fluorescence spectroscopy: A realistic potential curve of the Jahn−Teller distortion. J Am Chem Soc 129:5248–5256. https://doi.org/10.1021/ja069300s
256. Whitaker W, Sazanovich IV, Kwon Y et al (2023) Characterization of the reversible intersystem crossing dynamics of organic photocatalysts using transient absorption spectroscopy and time-resolved fluorescence spectroscopy. J Phys Chem A 127:10775–10788. https://doi.org/10.1021/acs.jpca.3c04780
257. Dias FB, Penfold TJ, Monkman AP (2017) Photophysics of thermally activated delayed fluorescence molecules. Methods Appl Fluoresc 5:012001. https://doi.org/10.1088/2050-6120/aa537e
258. Li G, Zhu Z-Q, Chen Q et al (2019) Metal complex based delayed fluorescence materials. Org Electron 69:135–152. https://doi.org/10.1016/j.orgel.2019.02.022
259. Zhang Y, Petersen JL, Milsmann C (2016) A luminescent Zirconium(IV) complex as a molecular photosensitizer for visible light photoredox catalysis. J Am Chem Soc 138:13115–13118. https://doi.org/10.1021/jacs.6b05934
260. Zhang Y, Lee TS, Petersen JL et al (2018) A Zirconium photosensitizer with a long-lived excited state: Mechanistic insight into photoinduced single-electron transfer. J Am Chem Soc 140:5934–5947. https://doi.org/10.1021/jacs.8b00742
261. Zhang Y, Petersen JL, Milsmann C (2018) Photochemical C–C bond formation in luminescent Zirconium complexes with CNN pincer ligands. Organometallics 37:4488–4499. https://doi.org/10.1021/acs.organomet.8b00388
262. Zhang Y, Akhmedov NG, Petersen JL et al (2019) Photoluminescence of seven-coordinate Zirconium and Hafnium complexes with 2,2′-Pyridylpyrrolide ligands. Chem Eur J 25:3042–3052. https://doi.org/10.1002/chem.201804671
263. Allen AR, Noten EA, Stephenson CRJ (2022) Aryl transfer strategies mediated by photoinduced electron transfer. Chem Rev 122:2695–2751. https://doi.org/10.1021/acs.chemrev.1c00388
264. Liu Q, Huo C, Fu Y et al (2022) Recent progress in organophotoredox reaction. Org Biomol Chem 20:6721–6740. https://doi.org/10.1039/D2OB00807F
265. Wu S, Schiel F, Melchiorre P (2023) A general light-driven organocatalytic platform for the activation of inert substrates. Angew Chem Int Ed 62:e202306364. https://doi.org/10.1002/anie.202306364
266. Weick F, Hagmeyer N, Giraud M et al (2023) Reductive activation of aryl chlorides by tuning the radical cation properties of N-Phenylphenothiazines as organophotoredox catalysts. Chem Eur J 29:e202302347. https://doi.org/10.1002/chem.202302347
267. Sartor SM, McCarthy BG, Pearson RM et al (2018) Exploiting charge-transfer states for maximizing intersystem crossing yields in organic photoredox catalysts. J Am Chem Soc 140:4778–4781. https://doi.org/10.1021/jacs.8b01001
268. Treat NJ, Sprafke H, Kramer JW et al (2014) Metal-free atom transfer radical polymerization. J Am Chem Soc 136:16096–16101. https://doi.org/10.1021/ja510389m
269. Discekici EH, Treat NJ, Poelma SO et al (2015) A highly reducing metal-free photoredox catalyst: design and application in radical dehalogenations. Chem Commun 51:11705–11708. https://doi.org/10.1039/C5CC04677G
270. Jin S, Dang HT, Haug GC et al (2020) Visible light-induced borylation of C–O, C–N, and C–X bonds. J Am Chem Soc 142:1603–1613. https://doi.org/10.1021/jacs.9b12519
271. Li P, Deetz AM, Hu J et al (2022) Chloride oxidation by one- or two-photon excitation of N-Phenylphenothiazine. J Am Chem Soc 144:17604–17610. https://doi.org/10.1021/jacs.2c07107
272. Du Y, Pearson RM, Lim C-H et al (2017) Strongly reducing, visible-light organic photoredox catalysts as sustainable alternatives to precious metals. Chem Eur J 23:10962–10968. https://doi.org/10.1002/chem.201702926
273. Cowper NGW, Chernowsky CP, Williams OP et al (2020) Potent reductants via electron-primed photoredox catalysis: Unlocking aryl chlorides for radical coupling. J Am Chem Soc 142:2093–2099. https://doi.org/10.1021/jacs.9b12328
274. Qian L, Shi M (2023) Contemporary photoelectrochemical strategies and reactions in organic synthesis. Chem Commun 59:3487–3506. https://doi.org/10.1039/D3CC00437F
275. Ghosh I, Ghosh T, Bardagi JI et al (2014) Reduction of aryl halides by consecutive visible light-induced electron transfer processes. Science 346:725–728. https://doi.org/10.1126/science.1258232
276. Ghosh I, Shaikh RS, König B (2017) Sensitization-initiated electron transfer for photoredox catalysis. Angew Chem Int Ed 56:8544–8549. https://doi.org/10.1002/anie.201703004
277. Xu J, Cao J, Wu X et al (2021) Unveiling extreme photoreduction potentials of donor–acceptor cyanoarenes to access aryl radicals from aryl chlorides. J Am Chem Soc 143:13266–13273. https://doi.org/10.1021/jacs.1c05994
278. MacKenzie IA, Wang L, Onuska NPR et al (2020) Discovery and characterization of an acridine radical photoreductant. Nature 580:76–80. https://doi.org/10.1038/s41586-020-2131-1
279. Christensen JA, Phelan BT, Chaudhuri S et al (2018) Phenothiazine radical cation excited states as super-oxidants for energy-demanding reactions. J Am Chem Soc 140:5290–5299. https://doi.org/10.1021/jacs.8b01778
280. Zhou J, Mao L, Wu M-X et al (2022) Extended phenothiazines: synthesis, photophysical and redox properties, and efficient photocatalytic oxidative coupling of amines. Chem Sci 13:5252–5260. https://doi.org/10.1039/D2SC01086K
281. Mayer L, Müller TJJ (2021) 3,10-Diaryl Phenothiazines – one-pot synthesis and conformational tuning of ground and excited state electronics. Eur J Org Chem 2021:3516–3527. https://doi.org/10.1002/ejoc.202100659
282. Clarke D, Gilbert BC, Hanson P (1976) Heterocyclic free radicals . Part VI. Substituent effects on the distribution of the spin density in 10-arylphenoxazine and 10-arylphenothiazine cation radicals. J Chem Soc, Perkin Trans. https://doi.org/10.1039/P2976000011 4
283. Vavilov S (1924) The fluorescence efficiency of dye solutions. Z Phys 22:266–272

284. Demchenko AP (2002) The red-edge effects: 30 years of exploration. Luminescence 17:19–42. https://doi.org/10.1002/bio.671
285. Kreutzer J (2025) Tune in for maximum reactivity. Nat Rev Chem 9:576–576. https://doi.org/10.1038/s41570-025-00755-x
286. Swain J, Mishra AK (2016) Nile red fluorescence for quantitative monitoring of micropolarity and microviscosity of pluronic F127 in aqueous media. Photochem Photobiol Sci 15:1400–1407. https://doi.org/10.1039/c6pp00123h
287. Krishna MMG (1999) Excited-state kinetics of the hydrophobic probe Nile red in membranes and micelles. J Phys Chem A 103:3589–3595. https://doi.org/10.1021/jp984620m
288. Marschner DE, Kamm PW, Frisch H et al (2020) Photocycloadditions in disparate chemical environments. Chem Commun 56:14043–14046. https://doi.org/10.1039/D0CC03911J
289. Kim SF, Schwarz H, Jurczyk J et al (2024) Mechanistic investigation, wavelength-dependent reactivity, and expanded reactivity of N–Aryl azacycle photomediated ring contractions. J Am Chem Soc 146:5580–5596. https://doi.org/10.1021/jacs.3c13982
290. Maafi M (2024) Excitation wavelength-dependent photochemistry. Photochem 4:233–270. https://doi.org/10.3390/photochem4020015
291. Kimura Y, Fukuda M, Suda K et al (2010) Excited state intramolecular proton transfer reaction of 4′-N,N-Diethylamino-3-hydroxyflavone and solvation dynamics in room temperature ionic liquids studied by Optical Kerr gate fluorescence measurement. J Phys Chem B 114:11847–11858. https://doi.org/10.1021/jp105033q
292. Suda K, Terazima M, Kimura Y (2012) Excitation wavelength dependence of photo-induced intramolecular proton transfer reaction of 4′-N,N-diethylamino-3-hydroxyflavone in various liquids. Chem Phys Lett 531:70–74. https://doi.org/10.1016/j.cplett.2012.02.004
293. Suda K, Terazima M, Sato H et al (2013) Excitation wavelength dependence of excited state intramolecular proton transfer reaction of 4′-N,N-Diethylamino-3-hydroxyflavone in room temperature ionic liquids studied by Optical Kerr gate fluorescence measurement. J Phys Chem B 117:12567–12582
294. Fukuda M, Terazima M, Kimura Y (2008) Study on the excited state intramolecular proton transfer of 4′-N,N-diethylamino-3-hydroxyflavone in imidazolium-based room temperature ionic liquids. Chem Phys Lett 463:364–368. https://doi.org/10.1016/j.cplett.2008.08.070
295. Lee S-K, Mills A, O'Rourke C (2017) Action spectra in semiconductor photocatalysis. Chem Soc Rev 46:4877–4894. https://doi.org/10.1039/C7CS00136C
296. Reeves JA, De Alwis Watuthanthrige N, Boyer C et al (2019) Intrinsic and catalyzed photochemistry of Phenylvinylketone for wavelength-sensitive controlled polymerization. ChemPhotoChem 3:1171–1179. https://doi.org/10.1002/cptc.201900052
297. Ghosh I, König B (2016) Chromoselective photocatalysis: controlled bond activation through light-color regulation of Redox potentials. Angew Chem Int Ed Engl 55:7676–7679. https://doi.org/10.1002/anie.201602349
298. Reiß B, Hu Q, Riedle E et al (2021) The dependence of chemical quantum yields of visible light Photoredox catalysis on the irradiation power. ChemPhotoChem 5:1009–1019. https://doi.org/10.1002/cptc.202100090
299. Lunic D, Bergamaschi E, Teskey CJ (2021) Using light to modify the selectivity of transition metal catalysed transformations. Angew Chem Int Ed Engl 60:20594. https://doi.org/10.1002/anie.202105043
300. Kerzig C, Wenger OS (2019) Reactivity control of a photocatalytic system by changing the light intensity. Chem Sci 10:11023–11029. https://doi.org/10.1039/C9SC04584H
301. Kurttila M, Camacho IS, Zitti A et al (2026) Environmental dipolar relaxation during excited-state proton transfer in Green Fluorescent Protein. J Am Chem Soc 148:7544–7551. https://doi.org/10.1021/jacs.5c21097
302. Lahm MT, Rauthe P, Fan K-C et al (2025) ICG revisited: excited-state dynamics as a function of dye concentration and solvent environment. Dalton Trans 54:15406–15415. https://doi.org/10.1039/D5DT01894C
303. Mauri A, Kiefer P, Neidinger P et al (2024) Two- and three-photon processes during photopolymerization in 3D laser printing. Chem Sci 15:12695–12709. https://doi.org/10.1039/D4SC03527E
304. Barner-Kowollik C, Bastmeyer M, Blasco E et al (2017) 3D laser micro- and nanoprinting: challenges for chemistry. Angew Chem Int Ed Engl 56:15828–15845. https://doi.org/10.1002/anie.201704695
305. Fischer J, Mueller JB, Quick AS et al (2015) Exploring the mechanisms in STED-enhanced direct laser writing. Adv Opt Mater 3:221–232. https://doi.org/10.1002/adom.201400413
306. Schafer KJ, Hales JM, Balu M et al (2004) Two-photon absorption cross-sections of common photoinitiators. J Photochem Photobiol A Chem 162:497–502. https://doi.org/10.1016/S1010-6030(03)00394-0
307. Li L, Gattass RR, Gershgoren E et al (2009) Achieving λ/20 resolution by one-color initiation and deactivation of polymerization. Science 324:910–913. https://doi.org/10.1126/science.1168996
308. Thielemann DT, Klinger M, Wolf TJA et al (2011) Novel Lanthanide-based polymeric chains and corresponding ultrafast dynamics in solution. Inorg Chem 50:11990–12000
309. Knöfel ND, Schweigert C, Feuerstein TJ et al (2018) Dimolybdenum paddlewheel as scaffold for heteromultimetallic complexes: Synthesis and photophysical properties. Inorg Chem 57:9364–9375. https://doi.org/10.1021/acs.inorgchem.8b01334
310. Valdmanis JA, Fork RL, Gordon JP (1985) Generation of optical pulses as short as 27 femtoseconds directly from a laser balancing self-phase modulation, group-velocity dispersion, saturable absorption, and saturable gain. Opt Lett 10:131–133. https://doi.org/10.1364/OL.10.000131
311. Niu S, Wang W, Liu P et al (2024) Recent advances in applications of ultrafast lasers. Photonics 11:857. https://doi.org/10.3390/photonics11090857